The Astrophysical Journal, 740:71 (15pp), 2011 October 20 doi:10.1088/0004-637X/740/2/71

DETECTIONS OF FAINT Lyα EMITTERS AT $z = 5.7$: GALAXY BUILDING BLOCKS AND ENGINES OF REIONIZATION*

Alan Dressler[1], Crystal L. Martin[2], Alaina Henry[2], Marcin Sawicki[3], and Patrick McCarthy[1]
[1] Carnegie Observatories, 813 Santa Barbara St., Pasadena, CA 91101-1292, USA; dressler@obs.carnegiescience.edu
[2] Department of Physics, University of California, Santa Barbara, CA 93106, USA
[3] Department of Astronomy and Physics, St. Mary's University, 923 Robie Street, Halifax, N. S., B3H 3C3, Canada; sawicki@ap.smu.ca
Received 2011 March 23; accepted 2011 July 20; published 2011 September 30

ABSTRACT

We report results of an unprecedentedly deep, blind search for Lyα emitters (LAEs) at $z = 5.7$ using the Inamori-Magellan Areal Camera & Spectrograph (IMACS), with the goal of identifying missing sources of reionization that could also be basic building blocks for today's L^* galaxies. We describe how improvements in wide field imaging with the Baade telescope, upgrades to IMACS, and the accumulation of ∼20 hr of integration per field in excellent seeing led to the detection of single-emission-line sources as faint as $F \approx 2 \times 10^{-18}$ erg s^{-1} cm^{-2}, a sensitivity five times deeper than our first search. A reasonable correction for foreground interlopers implies a steep rise of approximately an order of magnitude in source density for a factor of four drop in flux, from $F = 10^{-17.0}$ erg s^{-1} cm^{-2} to $F = 10^{-17.6}$ (2.5×10^{-18}) erg s^{-1} cm^{-2}. At this flux the putative LAEs have reached a surface density of ∼1 arcmin^{-2}—a comoving volume density of 4×10^{-3} Mpc^{-3}, several times the density of L^* galaxies today. Such a population of faint LAEs would account for a significant fraction of the critical flux density required to complete reionization at this epoch, and would be good candidates for building blocks of stellar mass $\sim 10^8$–10^9 $M_\odot$ for the young galaxies of this epoch.

Key words: dark ages, reionization, first stars – galaxies: formation – galaxies: high-redshift – galaxies: luminosity function, mass function

1. INTRODUCTION

It is known, from the observed polarization of the cosmic microwave background (Dunkley et al. 2009; Komatsu et al. 2009), that reionization of neutral hydrogen in the intergalactic medium (IGM) started at $z \gtrsim 8$ and, from the spectra of high-redshift quasars (Fan et al. 2002), was largely complete by $z \sim 6$. However, the formulation of a detailed picture describing, for example, when reionization began and how rapidly it proceeded, remains in an early stage. Even the source of the ionizing photons has not been *definitively* identified, although star-forming galaxies are the favored candidates.

Efforts to demonstrate whether galaxies can produce sufficient Lyman-continuum radiation to maintain an ionized IGM began with the discovery of galaxies at $z \sim 6$ (Bouwens et al. 2004; Bunker et al. 2004; Dickinson et al. 2004; Yan & Windhorst 2004) and the identification of this redshift as the epoch when reionization was completed (from Gunn-Peterson troughs in quasar spectra; see Fan et al. 2002, 2006). It was quickly recognized that the observed galaxies do not produce enough ionizing photons at $z \sim 6$ to balance the recombination rate in the IGM. However, this interpretation is complicated by the difficulty of predicting the ionizing output of galaxies from their 1500 Å UV continuum (Steidel et al. 2001; Shapley et al. 2006; Malkan et al. 2003; Siana et al. 2007, 2010; Cowie et al. 2009; Iwata et al. 2009; Vanzella et al. 2010; Nestor et al. 2011) and of estimating the clumpiness of the IGM (Madau et al. 1999; Pawlik et al. 2009) at these early epochs. Regardless, galaxies that are fainter than the limits of current surveys surely exist, and could in fact be the dominant source of ionizing photons (Bunker et al. 2004; Yan & Windhorst 2004; Trenti et al. 2010; Salvaterra et al. 2011).

Quantifying faint populations that remain undetected is crucial if we are to determine whether star-forming galaxies reionized the IGM. The most efficient way to find the faintest galaxies is to search for their strong Lyα emission, because such galaxies can be detected even when their stellar continuum radiation is fainter than the detection limit of the deepest *Hubble Space Telescope* (*HST*) surveys. Cowie & Hu (1998) pioneered the effort of using a narrow-band filter to find $z \sim 3$ Lyα emitting galaxies (LAEs). More than a decade later newer surveys have succeeded at higher redshifts and taken advantage of large telescopes with larger fields of view, notably Suprime-Cam on the Subaru telescope (Miyazaki et al. 2002). Large samples have been compiled for LAEs at $z = 5.7$ and 6.5, where Lyα emission is redshifted into "windows" of the OH airglow spectrum centered at $\lambda \approx 8200$ Å and $\lambda \approx 9200$ Å (Malhotra & Rhoads 2002, 2004; Shimasaku et al. 2006; Kashikawa et al. 2006, 2011; Hu et al. 2004, 2010; Ouchi et al. 2008, 2010). Nevertheless, only a fraction of these narrow-band imaging selected sources have been spectroscopically confirmed.

The contribution of LAEs to the ionizing photon budget has been debated. At $z \sim 3$ only 25% of star-forming Lyman break galaxies (LBGs) have Lyα emission with an equivalent width (EQW) large enough to be included in narrow-band samples (Shapley et al. 2003; cf. Steidel et al. 2011). However, the prevalence of Lyα emission in LBG samples appears to grow with increasing redshift. This was initially implied by the different evolutionary paths of the Lyα luminosity function (LF) of LAEs (Ouchi et al. 2008) and the UV LF of LBGs (Bouwens et al. 2007). Spectroscopic followup of $z \sim 4$–6 LBGs by Stark et al. (2010, 2011) seems to support this interpretation, but Douglas et al. (2010) reach a different conclusion. Regardless, if the Lyman-continuum emission is higher in LAEs than their LBG counterparts (as suggested by Iwata et al. 2009, Inoue et al. 2011, and Nestor et al. 2011), then observations could ultimately prove that LAEs dominate the reionization. Therefore, it is

* This paper includes data gathered with the 6.5 m Magellan Telescopes located at Las Campanas Observatory, Chile.

especially important to quantify the faint end of the Lyα LF back into the epoch of reionization.

Finding faint LAEs at $z \sim 6$ requires a new approach to reach fainter than is possible with narrow-band imaging. Spectroscopic searches accomplish this by dispersing the sky spectrum and observing at a spectral resolution that is close to the width of the emission line. Emission-line searches have now been carried out using a long-slit (Rauch et al. 2008), serendipitously (Sawicki et al. 2008; Lemaux et al. 2009; Cassata et al. 2011), and multi-slit "venetian-blind" masks (Martin & Sawicki 2004; Tran et al. 2004). In Martin et al. (2008, hereinafter Martin08), we presented the first sample of three $z \sim 6$ LAEs to be found by this multi-slit method and confirmed as LAEs in follow-up spectroscopy. These observations reached depths comparable to the narrow-band imaging surveys at this redshift (Ouchi et al. 2008; Murayama et al. 2007; Shimasaku et al. 2006; Hu et al. 2010), and they demonstrated that a fainter survey could be carried out.

We have now completed a deeper search for LAEs at $z = 5.7$ and achieved a sensitivity about five times better than our previous survey (Martin08). Among our candidates are many low-luminosity LAEs—only a few such objects have been discovered previously, via the technique of strong lensing by rich clusters of galaxies (Santos et al. 2004). We present the initial results of this search, principally a steep rise in the number of LAE candidates to faint fluxes. In Section 2 we describe improvements in our observational search with the Inamori-Magellan Areal Camera and Spectrograph (IMACS) that led to marked improvement compared to our earlier efforts. In Section 3 we describe the data used in this study, and in Section 4, we derive source counts for detected objects that show a steep rise in faint single-line sources. In Section 5 we present evidence, based on angular correlation functions and subtraction of known foreground populations, that a significant fraction of these faint sources are in fact LAEs. In Section 6 we discuss the implications of this result for the issues of early generations of star formation, the building blocks of the first galaxies, and the sources of cosmic reionization.

We adopt cosmological parameters of $\Omega_m = 0.30, \Omega_\Lambda = 0.7$, and $H_0 = 70$ km s^{-1} Mpc^{-1} throughout.

2. IMPROVEMENTS IN OUR NBMS MEASUREMENTS

The technique of "multi-slit narrow-band spectroscopy" (MNS) was pioneered by Crampton & Lilly (1999) and Martin & Sawicki (2004). We developed the technique for IMACS starting in 2004, conducting a search in both 2004 and 2005 in two fields, a 10h field in area of the COSMOS Survey (Scoville et al. 2007), and the other a 15h field from the Las Campanas Infrared Survey (LCIRS; Marzke et al. 1999). We used a "venetian-blind" mask with 1.″5 wide slits that covered the full $\approx$28′ diameter field of the IMACS $f/2$ camera with a filling factor of 10%. In that first application of MNS, we accumulated 5–10 hr of integration at two positions in each of these two fields, in photometric conditions that produced a point-source image size of $\sim$0.″8 FWHM. Further details of the observational setup are given in Martin08.

Our motivation for using the MNS technique was to carry out a deeper Lyα search than had been reached with narrow-band imaging, $F = 10^{-17}$ erg s^{-1} cm^{-2}, the limiting flux that was reached in the Subaru Deep Field (SDF; Shimasaku et al. 2006), corresponding to a magnitude in the narrow-band filter NB816 filter of NB816$_{\rm AB} = 26.0$. The depth advantage of MNS can be understood by comparing how sky background affects the limiting flux of source detection. With our MNS technique, a source is superposed on the dispersed sky background, which for typical LAEs is 10–15 Å of spectrum. In comparison, a narrow-band detection must compete against sky background approximately 10 times greater. Using the 2008 MNS exposures discussed here, we found that, for a source $F = 10^{-17}$ erg s^{-1} cm^{-2}, summed over 2″ in the spatial direction and the $\sim$120 Å FWHM bandpass of the NB816 filter, the ratio of counts (detected photoelectrons) $N_{\rm sky}/N_{\rm obj} \approx 100$. Thus, going fainter than this limit requires exceeding the precision of 1% photometry. Stubbs & Tonry (2006) describe in detail why, for standard *ground-based* observations with CCD detectors, achieving better than 1% photometry precision is not possible in practice.[4] The hardness of this limit can be appreciated by inspecting Figure 1 of Takahashi et al. (2007), which shows the rapid rise in photometric errors as NB816$_{\rm AB} = 26.0$ is approached. By reducing the sky background to what is effectively a narrower bandpass of 10–15 Å, our MNS observations with IMACS reach a line flux an order-of-magnitude deeper before this photometric limit is reached.

Our initial attempt successfully demonstrated MNS with IMACS and was the first time high-redshift LAEs had actually been detected with the technique. However, our first survey had not reached any fainter than the limit of narrow-band imaging surveys, which have the considerable advantage of covering large areas efficiently. We learned that a number of performance issues were responsible for limiting the sensitivity of our first search well below the potential of the technique. During the next two years, as we made follow-up observations for the three Lyα detections and other candidates presented in Martin08, we worked to improve several aspects of the system in an attempt to reach the project's original goal of $F \approx 3 \times 10^{-18}$ erg s^{-1} cm^{-2}. Because of the unusual gain in sensitivity of a factor of $\sim$5 between our earlier survey and the 2008 survey reported here, we briefly describe these improvements.

1. An undetected misalignment of Magellan-Baade wide-field atmospheric-dispersion-compensating (ADC) corrector delivered a significantly tilted focal plane to IMACS until 2007. This resulted in aberrated images for IMACS and also prevented the active optics system, which relies on the IMACS guiders, to provide accurate information to correct primary mirror shape, telescope collimation, and focus, and to accurately control telescope tracking. Once the ADC corrector was properly aligned, the performance of the system improved dramatically.
2. The "as-built" optics of the IMACS $f/2$ camera limited image quality to about 0.″7 FWHM over the 1/2° field, compared to the specification of a 0.″35 FWHM contribution to the image point-spread function (psf). Tests performed in 2007 showed that a field-dependent coma was mainly responsible, with additional degradation from focal plane tilt and astigmatism. Optical modeling led to a repositioning of the field flattener in order to cancel the coma and reduce astigmatism (see Dressler et al. 2011 for a full description). Though a difficult modification at that stage of the IMACS operation, the resulting adjustments returned the camera to performance close to original specifications: in the best seeing (psf $\leqslant$0.″35 FWHM), the $f/2$ camera produces 0.″50 FWHM images over 85% of field.

[4] Systematic errors of ground-based observations—chief among them, flat-fielding errors due to differences in the energy distributions of "flats," (time-dependent) sky, and sources—limits precision to 1% at best unless "chopping" techniques are employed.

3. With the substantial help of a 2006 NSF *TSIP* award, the original CCD Mosaic camera at the $f/2$ focus was replaced by a new one using E2V detectors. This raised the system throughput (including telescope) from 14% to 22% at 8200 Å, a factor of 1.6 gain.
4. The first four nights of a five-night observing run with IMACS for this program, 2008 April 8–12, were excellent: clear, with seeing of typically 0.45–0.55 arcsec *on the detector*, and with perfect performance of telescope and instrument. The quality of the data collected on these nights far surpassed that of the 2004–2005 data.

3. DATA AND DATA REDUCTION

Our observational setup in 2008 followed that of our earlier Lyα search, described in Martin08. One new slit mask was fabricated for the 10h field; the new search mask copied the original design of 100 parallel slits of width 1.″5 and a center-to-center spacing of 15″. As before, this layout sampled 10% of the IMACS $f/2$ field. A custom narrow-band filter centered at 8190 Å with a designed FWHM $\Delta\lambda \approx 150$ Å was mounted in the IMACS pupil directly in front of the 200 l mm^{-1} grism. This configuration produces 100 spectra, at a dispersion of 2.0 Å pixel^{-1}, and a projected 1.″5 slit width of 6 pixels. The spectra overlap slightly in wavelength, and there is a zero-order image of the slit mask (and field) that covers much of the lower half (chips 1–4) of the CCD mosaic, complicating the reduction. A small amount of sky coverage is also lost because of metal bridges ("tines") that stiffen the mask against warping by dividing the long slits into discrete sections. After accounting for these obstructions, the actual on-sky area is 55.3 arcmin^2 per exposure. A schematic of the search mask is shown in Figure 2 of Martin08.

Over the nights 2008 April 8–12, 24 frames were taken in the 10h COSMOS field (10:00:43, 02:11:00 [2000]) and 23 in the 15h LCIRS (15:23:35, −00:08:00 [2000]) field, for a total exposure of 18.75 and 22.75 hr, respectively. For each night's exposure there was a slight drift of the slit mask pattern over the detector, about 5 pixels along the dispersion and 2 pixels across, that accumulated as the field was tracked from several hours east to several hours west of the meridian. After dome flats were used to correct the pixel-to-pixel sensitivity variations of the detectors, these frames were shifted before stacking to form a single, very deep exposure for each of the two fields. Because this was a blind search, object positions were not known a priori, so the IMACS data reduction package COSMOS[5] could not be used at this stage. Instead, a set of IRAF scripts were developed, the most important of which was a "running average" of ±10 columns (the dispersion direction) that provided a mean sky spectrum to subtract sky from each of the 100 long-slit spectral "bands" (short in wavelength, long on the sky). This worked well, although it was recognized that more accurate sky subtraction would need to be redone later—after object identification—because the sky determined with the running-average technique is necessarily biased by as-yet-unidentified objects that are included in the averages.

Because of the high number of artifacts and non-astronomical "features" on these unconventional data frames, we chose to search by eye for emission-line objects, with and without continuum to the blue of the emission. C.L.M., A.D., and P.M. independently examined both fields, compiling lists that separated the detections into four categories: (1) clear single-emission-line (SEL) source without a blue continuum; (2) probable but not certain SEL source without a blue continuum; (3) single or multiple emission-lines source with a blue continuum;[6] (4) possible, low signal-to-noise ratio (S/N) detection of an emission line without a blue continuum. The last category had the largest source count and probably contained comparable numbers of real and spurious detections.

The sample used in this paper includes only those objects that are certainly real or very likely to be; almost all were originally placed by the three classifiers in classes (1) and (2). After cross-comparing and re-examining our individual lists, a final list of such candidates was assembled. The 10h field has 104 SEL sources without blue continua (80 class (1) sources and 24 class (2) sources) and 130 emission-line sources with blue continua. The 15h field has 111 SEL sources without blue continua (77 class (1) sources and 34 class (2) sources) and 105 emission-line sources with blue continua. We will call the latter "Em+C"—sources in this category are objects that are certainly foreground (including the few cases of multiple emission-line sources without a detectable continuum.) However, the single-emission-line sources without blue continua, which we will call SELs, are candidate LAEs. Figure 1 shows a mosaic of 5″ × 50 Å spectra for the SELs in the 10h COSMOS field, and Figure 2 shows the SELs in the 15h LCIRS field.

In Figure 3 we show the derived S/N for the sources shown in Figures 1 and 2. These were determined by adding up the flux in square apertures—1.″8 for sources brighter than, and 1.″4 for sources fainter than, $F = 10^{-17.5}$ (3.2×10^{-18}) erg s^{-1} cm^{-2}—and by estimating the noise from the much greater sky flux, determined separately for each of the two fields. (The choice of slightly smaller apertures for the fainter sources modestly reduces the scatter in S/Ns.) The plot confirms that incompleteness becomes substantial at log F erg s^{-1} cm^{-2} ≈ -17.6 (2.5×10^{-18} erg s^{-1} cm^{-2}), at which point the typical S/N ≈ 3. Although our selection was done visually, we were apparently successful in drawing the line with a relatively sharp cutoff in S/N. The implication, of course, is that there are many more real sources among the class 4 candidates, but also many that are statistical fluctuations and artifacts, as we supposed. In this paper we use a flux cut of log F (erg s^{-1} cm^{-2}) $\geqslant -17.6$.

Once the SEL and Em+C sources were identified, the COSMOS data reduction package could be used to make two-dimensional spectral extractions with accurate sky subtraction. Another COSMOS program, *viewspectra*, was used to examine the sky-subtracted two-dimensional spectrum in order to select the spectral "columns" containing the object. Generally, the extractions were 9 pixels centered on the object (1.″8), but some variation was made to optimize S/N for more diffuse or more compact objects, and to avoid artifacts that dot the frames. These one-dimensional spectra were then inspected with IRAF *splot* to make, if necessary, an adjustment to the continuum level, in order to measure the emission line over zero background, and to determine the wavelength limits for integrating the counts. Counts were summed and converted to flux by the calibration 1.35×10^{-20} erg s^{-1} cm^{-2} per IMACS count (photoelectron). The calibration came from six measurements of two Hamuy standard stars EG274 and LTT7379 (Hamuy et al. 1994) through a 7″ round aperture on two of the four nights, which were in

[5] http://www.obs.carnegiescience.edu/Code/cosmos

[6] A few multiple emission-line sources without blue continua were included in this category.

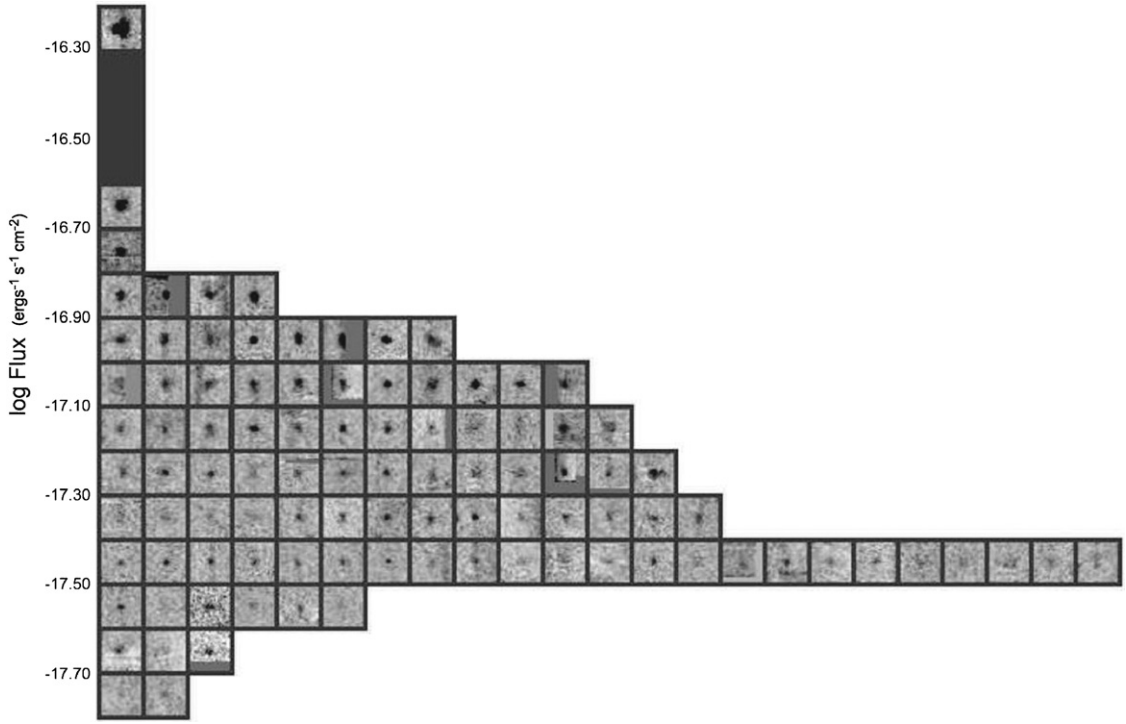

Figure 1. Mosaic of $5'' \times 50$ Å boxes (spatial—horizontal, wavelength—vertical) of the sample of SELs (single-emission-line without blue continuum) sources in the 10h (COSMOS) field. A flux of $F = 10^{-17}$ erg s^{-1} cm^{-2}, a natural limit for narrow-band photometric studies, is easily reached with these data, at the $\sim 10\sigma$ level. A flux of $F = 3 \times 10^{-18}$ erg s^{-1} cm^{-2} is detected at the $\sim 3\sigma$–4σ level. The number of sources rises rapidly with decreasing flux, as described in the text. Strong artifacts (e.g., cosmic rays, bad pixels, and sky subtraction problems) have been blanked out in some cases.

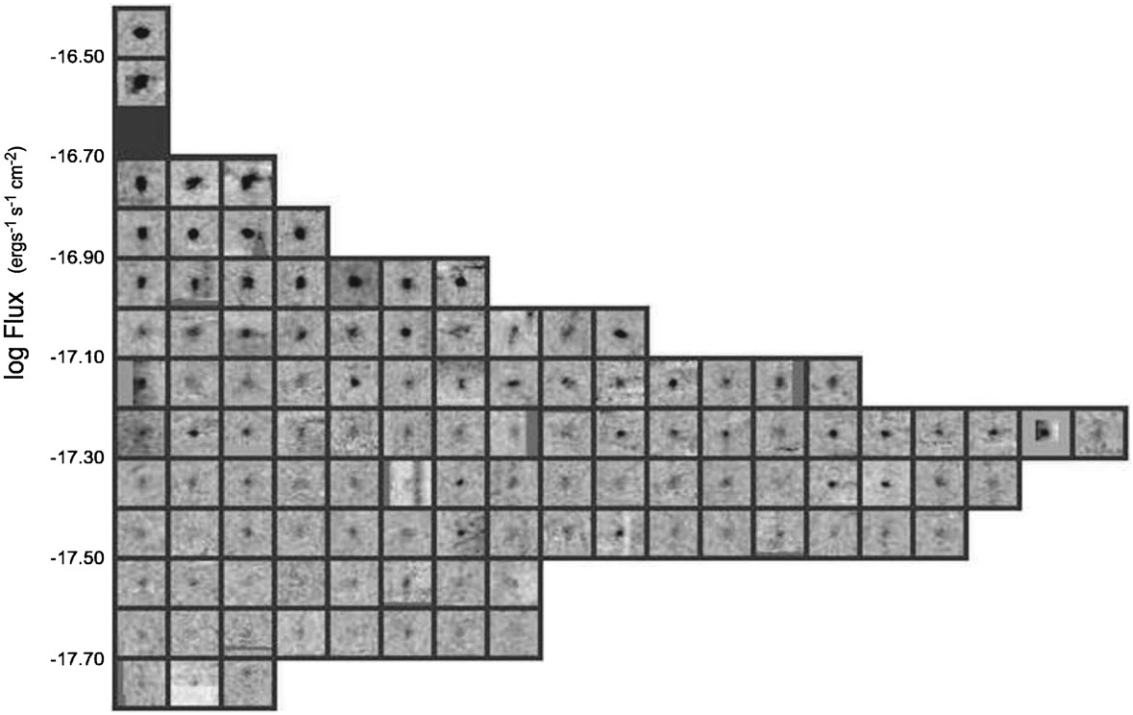

Figure 2. Same as Figure 1, for detected SEL sources in the 15h LCIRS field.

agreement to about 5%, a systematic error considerably larger than the photon statistics of the observations.

4. RESULTS OF THE SEARCH: DERIVATION OF SOURCE COUNTS

With measured fluxes for the SEL sources (presumed $z \sim 5.7$ LAEs or foreground emission-line galaxies) and fluxes for the Em+C sources (certain foreground galaxies), we plot in Figure 4 cumulative source counts versus measured flux. The blue line shows the cumulative distribution of all emission-line sources detected in the two fields. The black line shows the counts for SEL sources. The black line rises steeply, arguably more steeply than any known foreground population, as indicated, for example, by our own counts of foreground galaxies, the Em+C sources (the red line). (As we show in the next section,

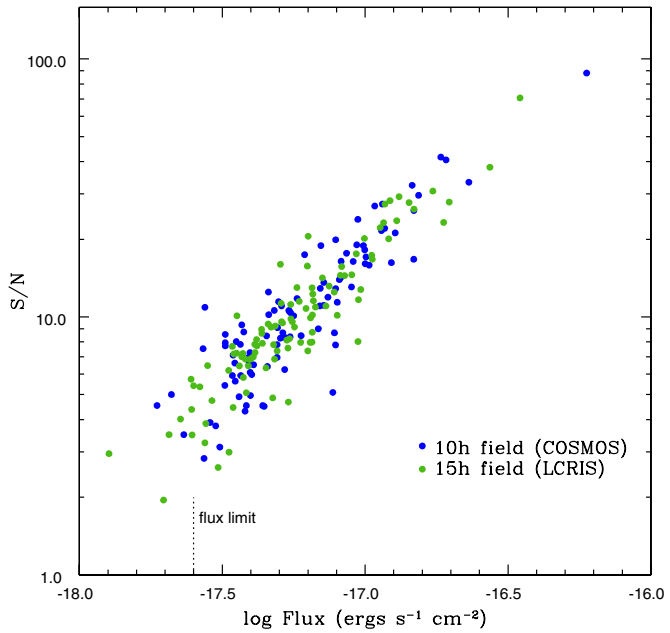

Figure 3. S/Ns for the detections displayed in Figures 1 and 2. Blue points: 10h field; green points: 15h field. The sample used in this paper is cut at log F (erg s^{-1} cm^{-2}) > -17.6 (2.5×10^{-18} erg s^{-1} cm^{-2}).

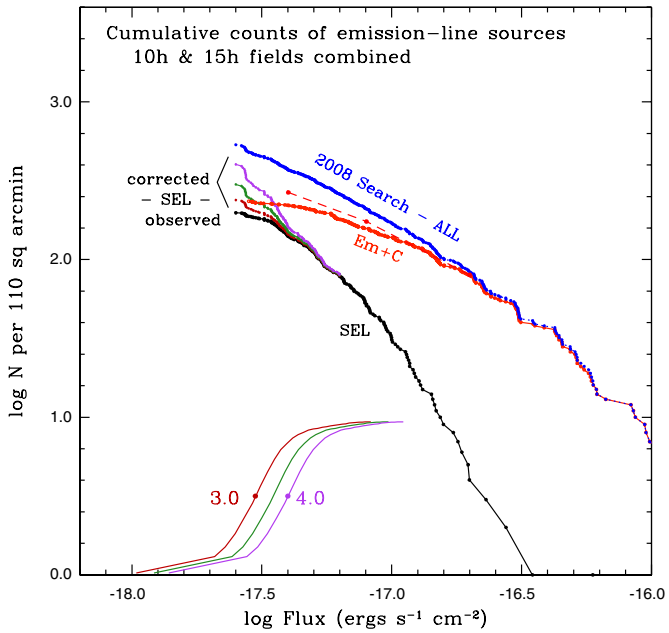

Figure 4. Cumulative source counts formed for both the 10h (COSMOS) and 15h (LCIRS) fields, in $\log_{10}$ number per 110 arcmin^2, the combined area surveyed in the two fields. The red line shows the cumulative counts of "Em+C" (emission-line sources with blue continua); the black line shows the counts of "SEL" (single-emission-line-only) sources. The faint end of the latter is shown in raw counts as well as after correction for three different values of the completeness correction (see the text), at 50% incompleteness levels of $F = 3.0$, 3.5, and 4.0×10^{-18} erg s^{-1} cm^{-2}. (The form of the incompleteness function is shown at the bottom of the figure, and the correction applied to the observed counts—the black line—is shown in red, green, and purple for the these three bounding values of the 50% completeness level.) The red line Em+C distribution has not been corrected for this incompleteness, but for a larger effect that results from the increasing difficulty of detecting a continuum for progressively fainter emission lines. The dashed red line is an estimate of the correction that is needed because of this effect. As explained in the text, the "ALL" line, a sum of the uncorrected Em+C counts and the SEL counts corrected for the "3.5" incompleteness, has instead been chosen as the basis for the subsequent analysis of the LAE luminosity function.

these are almost entirely [O II] emitters at $z \approx 1.19$, [O III] emitters at $z = 0.63$, and Hα at $z = 0.25$.) This is our first indication that many of the SEL sources are LAEs at $z = 5.7$. However, another possibility is that foreground galaxies that would otherwise be on the red line have been added to the black line, if we systematically fail to detect their continuum flux as we observe fainter sources of moderate EQW. For this reason, we cannot simply credit the steep rise in emission-line-only sources as exclusively or even *mainly* due to LAEs. We return to this issue below after discussing the incompleteness correction for the SEL counts.

As can be appreciated from the sharp peak in the emission-line-only sources in Figures 1 and 2, incompleteness in our SEL detections sets in sharply at $F \approx 3 \times 10^{-18}$ erg s^{-1} cm^{-2}. (This is seen in the cumulative counts of Figure 4 as the sudden leveling-off of the black line.) In Martin08, we investigated incompleteness by the technique of randomly inserting point sources of different flux levels and using SExtractor to try to recover these sources. The result of that experiment was just such a sharp cutoff, whose form is reproduced in Figure 4 for three different flux values of 50% incompleteness. When this form of the incompleteness correction is applied for 50% flux values of 3.0, 3.5, 4.0×10^{-18} erg s^{-1} cm^{-2}, we obtain the red, green, and purple extensions, respectively, to the black line of Figure 4. The result is very reasonable, extending the SEL source counts at roughly the same slope down to the limit of our detections, and constraining the 50% point to a small range. For the 2008 MNS search data, then, we adopt the Martin08 form and choose $F = 3.5 \times 10^{-18}$ as the flux where incompleteness falls to 50%. We emphasize that we use the incompleteness correction only to demonstrate that there is no evidence for a "turnover" in the SEL counts to the limit of our observations. Because the steep slope of the black line is well established before the small interval over which the incompleteness correction is applied, none of the results in this paper rely on applying this correction.

The incompleteness correction has not been applied to the Em+C source counts. (In fact, so few galaxies are being added to the Em+C counts at the limit of the survey that making the correction used for the SEL counts would add only about seven sources.) A more important incompleteness, one that sets in more gradually, comes from selecting the Em+C sources with a combination of continuum and line flux. The issue is that increasing numbers of the faintest foreground sources will not be identified as such if their stellar continua are too faint to be detected in our survey. These sources will not be lost, but will be added to the SEL counts if their emission-line fluxes are above the detection threshold. In order to estimate the magnitude of this problem, we measured EQW of 212 emission lines found in the Em+C sample and divided the sample into three flux ranges, $4 < F < 8$ (67), $8 < F < 20$ (76), and $20 < F < 1000$ (69), where F is the flux in units of 10^{-18} erg s^{-1} cm^{-2} (sample size in parentheses). We assume the brightest sample represents an intrinsic EQW distribution that is independent of emission-line flux. As expected, the two fainter distributions show a deficiency of higher EQWs: the median EQW drops from 66 Å for the brightest sample to 43 Å for the intermediate flux sample to 21 Å for the faint sample. From the faintest sample it is clear that incompleteness sets in at EQW $\gtrsim$ 50 Å; there are essentially no EQW $>$ 100 Å cases. Taking the conservative case of EQW = 50 Å as the detection limit for the medium and faint samples, we calculate that 47 sources are missing from the Em+C counts; presumably, these have been added to the

SEL sample. This simple modeling suggests that approximately 22% of the SEL sample are lower-flux foreground objects whose continuum is too faint to be detected. While significant, this is not a large fraction of SELs, so there must be higher EQW foreground sources (EQW $\gtrsim$ 500—missed even for our brightest sources) and/or genuine no-continuum sources, for example, LAEs, that dominate the SEL sample.

In Figure 4 we show the Em+C line as corrected for EQW incompleteness as the dashed red line. Because it unlikely that the EQW distribution is independent of luminosity, as we have been obliged to assume, this correction is not accurate enough to separate the LAE population from foreground galaxies. Therefore, we will not use the red line Em+C distribution, in raw or corrected form in the analysis that follows. Instead, we combine the uncorrected Em+C distribution with the SEL sources (corrected for incompleteness with 50% incompleteness at $F = 3.5 \times 10^{-18}$ erg s^{-1} cm^{-2})—this is the "ALL" emission-line sources seen in Figure 4 (the blue line). With this we will circumvent the uncertainty associated with detection of a faint continuum, by subtracting an independently derived foreground population from the combination of LAEs and foreground galaxies that together comprise the full MNS sample of emission-line sources.

5. ANALYSIS: IS THE STEEP RISE IN FAINT SEL SOURCES DUE TO LAEs AT $z = 5.7$?

Although it is certain that some of the rising SEL counts are LAEs at $z = 5.7$, the size and significance of this population depends on how many of these sources are foreground galaxies. A decisive answer to this question will come from higher resolution spectra of the fainter LAE candidates to distinguish, in particular, Lyα emission from [O II]—the common foreground contaminant that is most likely to appear as a single line at the spectral resolution of the 2008 search data. With a spectral resolution of a few angstroms, Lyα will often exhibit an asymmetric profile, sharply attenuated to the blue but with a red "wing," while the [O II] doublet lines will be resolved ($\Delta\lambda = 5.7$ Å for $z = 1.19$), thus providing a definitive test of the two most likely possibilities. The challenging task of obtaining a statistically significant sample of higher resolution spectroscopy for our fainter candidates is underway at the Keck and Magellan telescopes.

5.1. Using the COSMOS Data to Extrapolate Foreground Contamination

In lieu of decisive spectroscopic confirmation of faint LAEs, we explore what can be learned by a statistical subtraction of the foreground population. Our own observations of foreground Em+C galaxies, like our sample of SEL sources, are the faintest such sample available. However, as discussed above, our data themselves show that the faintest foreground sources are not identified as such when the stellar continuum is too weak to be detected.

To work around the problem—that the lack of a detected continuum for an SEL does not necessarily imply that this object is an LAE—we take advantage of a wider-area search for foreground emission-line galaxies by the COSMOS Survey, observations with Suprime-Cam that include numerous broad bands as well as intermediate- and narrow-band filters (Taniguchi et al. 2007). One in particular, the NB816 filter, covers a bandpass close to that used in our study: central wavelength $\lambda_c = 8150$ Å for NB816 compared to our $\lambda_c = 8185$ Å, and FWHM bandwidth $\Delta\lambda = 121$ Å compared to our $\Delta\lambda = 134$ Å. Combining narrow-band detections of emission-line sources with detections in several broad bands allows good discrimination into different redshift intervals, as described in Takahashi et al. (2007) and Shioya et al. (2008) (see also Ly et al. 2007). This much wider-area search for emission-line sources provides a sample of foreground galaxies that is populous enough to well constrain the LF. The COSMOS observations reach a limiting flux $F = 10^{-16.85}$ erg s^{-1} cm^{-2}, although—as discussed in Section 2—approaching this flux limit the uncertainty in these detections rises considerably. Nevertheless, the samples are large and uniform; they provide a solid database for determining foreground LFs that can be extrapolated to the flux limit of our LAE search.

Figure 5 shows the distribution of emission-line sources also detected in continuum bands, parsed into [O II] at $z \approx 1.19$, [O III] at $z \approx 0.63$, and Hα at $z \approx 0.25$.[7] For a sample this bright, almost all emission-line sources belong to one of these foreground populations. These data are extracted from the COSMOS Intermediate and Broadband Photometry Catalog;[8] emission-line galaxies are selected following the narrow-band excess method described in Takahashi et al. (2007). This sample provides the crucial advantage for our purposes that fluxes have *not* been corrected for internal extinction—correcting for extinction is commonly done because most studies have focused on the star formation rate over cosmic time.

The sample we extracted is centered on our 2008 search field, shown by the inner circle in Figure 5, and extending to a radius of 0.°7—most, but not all, of the area of the COSMOS NB816-excess catalog. The percentage compositions of [O II], [O III], and Hα for the larger area are 53%, 34%, and 13% respectively, and 55%, 32%, and 13% for the smaller area of the 2008 search. Figure 5 shows that [O II] at $z \approx 1.19$ is the major foreground and that, for these O II sources in particular, there is apparent large-scale structure—a prominent filament structure crosses the IMACS field. (The COSMOS photometric redshifts place this filament at $1.18 < z < 1.20$, within the bandpass of both the NB816 and our MNS narrow-band filter.) This feature offers the possibility of a simple test comparing the spatial distributions of LAE candidates and foreground emitters to estimate the degree of foreground contamination.

5.2. Evidence from Cross-correlation that Many of the Faint Sources are LAEs

The relatively strong filament of foreground [O II] emitters, the most numerous of the foreground sources, suggests that we might cross-correlate positions of [O II] sources in the COSMOS catalog to estimate what fraction of the candidate LAEs are instead members of this foreground. Although our sample of LAE candidates extends somewhat fainter, there is substantial overlap in the fluxes of the two samples.

We have made such a test by constructing angular correlation functions, various forms of which are discussed by Landy & Szalay (1993). In our particular application we cross-correlate the spatial positions of the SEL sources—candidate LAEs—with the largest foreground population, the sample of

[7] In fact, no broadband photometric criteria for selecting [O III] explicitly have been published in the COSMOS study. We have therefore taken the [O III] sample to be what remains of the NB816-excess (Δmag > 0.20) sample after removing the [O II] and Hα sources, which means there is also a smaller contribution of Hβ emitters ($z \approx 0.68$) in the [O III] sample. The Hα sample is likely to contain a similar contribution of [S II] sources.

[8] http://irsa.ipac.caltech.edu/Missions/cosmos.html

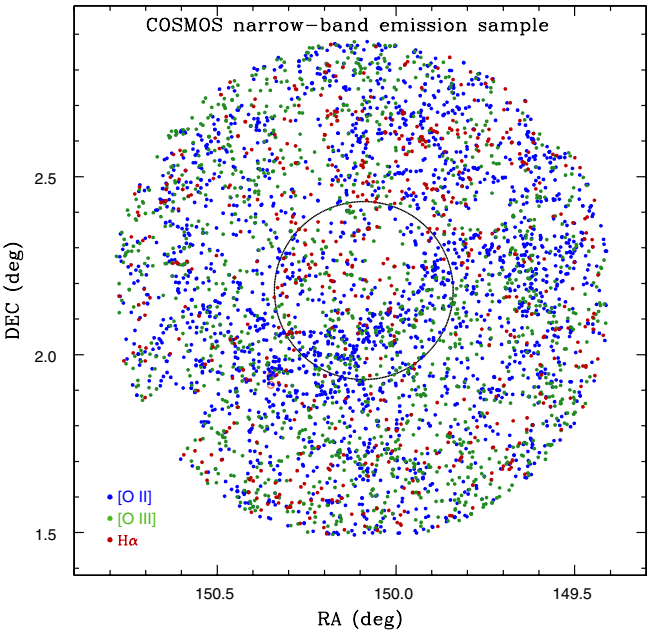

Figure 5. COSMOS Survey detections of emission-line galaxies with a blue continuum in the NB816 filter, which includes emission-line sources brighter than $F = 10^{-16.85}$ erg s^{-1} cm^{-2}. Components of this sample are [O II] emission at $z \approx 1.19$, [O III] at $z \approx 0.63$, and Hα at $z \approx 0.25$. The smaller circle is the IMACS field of our 2008 search; the larger circle, with a 0.°70 radius, is the area we used for determining the foreground contamination per area. (This is most but not all of the rectangular area of the NB816 catalog.) Large-scale structure in the distribution of foreground galaxies can be clearly seen, particularly for the [O II] emitters.

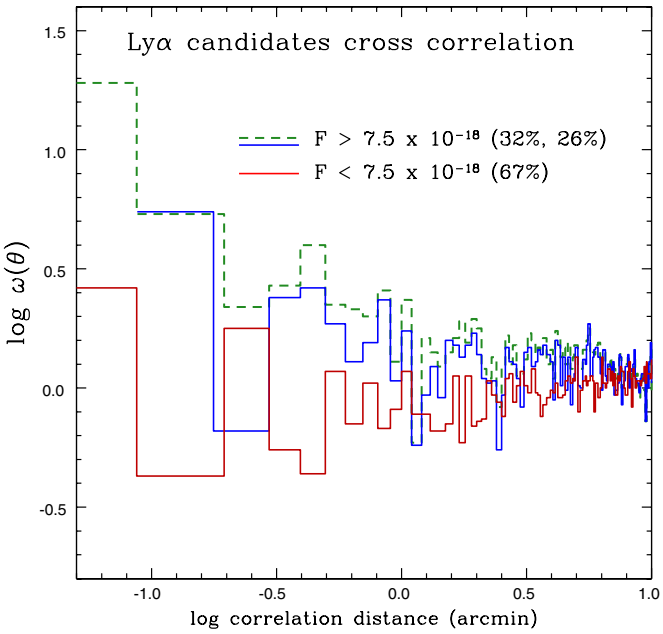

Figure 6. Angular cross-correlation function $\omega(\theta)$ between SEL sources found in our 2008 search of the 10h field and the COSMOS narrow-band detections of galaxies with [O II] emission at $z \approx 1.19$ over the full IMACS field. The dashed green line shows a very strong correlation between 33 bright SEL sources ($F > 7.5 \times 10^{-18}$ erg s^{-1} cm^{-2}) and foreground [O II] emitters, however, the strong signal in the first bin is due to the fact that six of these bright SEL sources are certain or probable H II regions in galaxies in the [O II] sample. However, even without these, the correlation function for the bright sample—the blue line—is still strong, a 4σ or greater difference from "random." In contrast, the red line shows that the 70 faint SEL sources ($F < 7.5 \times 10^{-18}$ erg s^{-1} cm^{-2}) are uncorrelated with the foreground [O II] emitters, suggesting the latter make up half or less of this population. Monte Carlo models show this result to be very significant as well, although the unavailability of a foreground population as faint as our sample prevents a good constraint on how big the foreground contribution can be. This decline in amplitude of the cross-correlation function with decreasing flux suggests that the steep rise in SEL sources is the result of a large population of LAEs at $z = 5.7$.

[O II] sources at $z \approx 1.19$ from the COSMOS Survey. Specifically, we measure the angular separation in arcminutes for all SEL–[O II] pairs and compare to expectations for randomized placements of the SEL sample over the search field. In the notation of Landy & Szalay, the angular cross-correlation function we use is $w(\theta) = (D_{\rm SEL} D_{\rm [O\,II]} / R_{\rm SEL} D_{\rm [O\,II]}) - 1$.

The results of the cross-correlation test are shown in Figure 6. We know from Martin08 and from the SDF search for LAEs (Shimasaku et al. 2006) that foreground dominates over LAEs by ∼5–10:1 for a sample with $F \gtrsim 10^{-17}$ erg s^{-1} cm^{-2}. Therefore, we divided the SEL sample of LAE candidates at $F = 7.5 \times 10^{-18}$ erg s^{-1} cm^{-2}—33 sources are brighter, and 71 are fainter than this value. The dashed green line in Figure 6 shows the result for the bright sample—a very strong correlation signal over the six bins of pair separations $R \leqslant 0.'6$. Over this interval 46 pairs are observed, compared to only 13 predicted for a random placement of the [O II] sources—statistically significant at more than 10σ. However, it is clear that this result is strongly driven by the smallest pair separations $\delta \leqslant 0.'1$, where there are seven pairs from six galaxies. Suspiciously, the largest of the separations was 1.″8, much smaller than the $\delta \leqslant 6''$ covered by this bin. After examining these with the *HST*-ACS images of the COSMOS field, we recognized that—as found in Martin08—three cases were certainly members (and the other three probable members) of the [O II] catalog with which we were correlating; that is, these SELs appear to be H II regions in the outer parts of foreground galaxies. On this basis we made a conservative choice to remove all six sources from the bright sample, leaving 27. Significantly, only one such close pair ($\delta = 1.''0$) was found for the 71 faint SEL sources (even fainter H II region of the same foreground galaxies should be detectable), which was similarly removed.

Figure 6 shows that the angular cross-correlation signal for the remaining bright sample of 27 remains significant, indicating that many of these SEL sources are foreground members at $z \approx 1.19$. With the central bin eliminated, there is still a clear signal—the blue line—for the five remaining bins that tally 24 pair separations up to 0.′6. Over this interval, only 11 pairs are predicted for a random spatial distribution of the 27 sources—a ∼7σ difference. In contrast, for the remaining 70 SELs with $F < 7.5 \times 10^{-18}$ erg s^{-1} cm^{-2}, there is no clear correlation signal over the same 6 bins: 28 are expected and 26 are found—this null result is also very significant, as we now demonstrate.

Monte Carlo simulations can be used to enhance this analysis and, in particular, to test whether the strength of the correlation or lack thereof is consistent with expectations. In our simulations we constructed simulated SEL samples of 27 and 70 by drawing randomly from the [O II] population and adding a number of randomly placed objects to simulate other objects. For example, we expect the majority of the SEL sample with $F > 7.5 \times 10^{-18}$ erg s^{-1} cm^{-2} to be foreground galaxies, and that roughly half of these should be [O II] emitters. Specifically, we tested for the 27 bright sources by making 1000 realizations in which we extracted 14 objects from the [O II] sample (removing them temporarily from that sample) and also placed 13 other objects at random positions to represent—in the proportions of the COSMOS narrow-band sources—nine O III and two Hα;

this simulation produces a mean number of 24 separations with $R \leqslant 0\farcs6$, the same as the 24 pairs of the observed sample and leaves room for two LAEs at $z = 5.7$. However, because of the small sample size, the simulations cannot well constrain the foreground or LAE fraction. For example, a mix of eight [O II] selections (plus six other foregrounds and 13 genuine LAEs) will also yield 24 pair separations $R \leqslant 0\farcs6$ at the 1σ level. Nonetheless, the case of *zero* foreground produces only four out of 1000 models with 24 or more pairs, a $> 3\sigma$ rejection that is at least qualitatively in agreement with the simple Poisson calculation done above. In summary, the bright 33 SEL sample is dominated by foreground objects, six that are identified as actual COSMOS sources, and—from the Monte Carlo models—between 58% (the 1σ lower limit) and 100% of the remaining 27 sources also foreground.

The Monte Carlo simulations are also effective in testing the significance of the null signal for the 70 candidate sample with $F < 7.5\times10^{-18}$ erg s^{-1} cm^{-2}. Adopting the same fractions as the "best-fit" case above—36 [O II] and 34 random ([O III], Hα, and LAE)—leads to a mean expectation value of 60 pairs for $R \leqslant 0\farcs6$, far exceeding the measured value of 26 for the observed 70 SEL sample—this "nearly all foreground case" appears to be ruled out at the $\sim4\sigma$ level. The "half-foreground" case, 19 [O II] and 16 [O II] and Hα, with a 50% population of LAEs, has a mean expected value to 46—still unacceptably large, although "26 pairs" is allowed at the 2σ level. To reach a 1σ level the foreground must be reduced to seven [O II] draws and six random placements. Taken at face value, then, the lack of a prominent signal in Figure 6 for the 70 faint source sample of candidate LAEs suggests that the foreground population should be less than 25%. This further suggests a very sharp change in foreground contamination which, anticipating the result of Section 5.4, would require an improbably steep rise in LAEs sources.

There is, however, a further issue to consider. The 27 source bright sample covers the same flux range as the COSMOS [O II] catalog, making a simple draw from the [O II] distribution a reliable way to test the expected strength of the correlation function. In contrast, the faint sample of 70 sources are all fainter than anything in the COSMOS catalog. In general, correlation functions are observed to depend on source luminosity (or mass) in the sense that higher-luminosity sources are more strongly clustered. We tested the likely strength of this effect by dividing the [O II] sample in half, split at $\log F$ (erg s^{-1} cm^{-2}) $= -16.57$. Returning to the "half-foreground" case, when we draw only from the brighter half of the [O II] sample, the Monte Carlo simulation predicts a mean expected number of 49 [O II] sources, while drawing from the faint sample the mean number drops to 40—a significant weakening of the correlation strength. If this trend continues to the yet-fainter 70 source sample, the "half-foreground" sample would be compatible with the weak cross-correlation signal between the faint sample of LAE candidates and the COSMOS [O II] foreground. While our samples of candidate LAEs are too small to accurately quantify this effect, its sign is clear. Unfortunately, this uncertainty makes it difficult to constrain the foreground contamination within the 0%–50% level, but the "nearly all foreground" case found for the bright sample remains highly unlikely. Recall also that only a single pair was removed from the sample of 70 faint sources as a likely H II region of the foreground [O II]-emitting population.

In summary, when the sample of 104 SELs in the 10h search field is divided into brighter/fainter than $F = 7.5\times10^{-18}$ erg s^{-1} cm^{-2}, the difference in strength of the angular cross-correlation with the [O II]-emitting foreground is highly significant. The strong signal observed for the brighter 33 SEL sample, even after removing six actual foreground objects, indicates that the majority of this sample is foreground and only a minority can be LAEs, consistent with previous studies. In contrast, the absence of a strong signal for the faint 70 SEL sample rules out the possibility that the most are foreground galaxies, indicating instead that approximately half are LAEs. This is our first good evidence that the rapid rise in the faint SEL counts is due to a substantial increase in the number of LAE emitters at $z = 5.7$, something we can investigate further by looking at the LFs of the foreground sources, information that is independent of their positions on the sky.

5.3. Fitting Schechter Luminosity Functions to the COSMOS Foreground Counts

With good measurements of the observed foreground populations of [O II], [O III], and Hα emitters with fluxes $F > 10^{-17}$ erg s^{-1} cm^{-2} from the COSMOS Survey, we proceed to use these counts to predict the foreground population down to the faintest levels of our survey, $F \sim 2.5\times10^{-18}$ erg s^{-1} cm^{-2}. This was accomplished by binning the observed counts and fitting Schechter functions (Schechter 1976). In general, this was a straightforward procedure, except for the case of [O II], which makes up more than half of the foreground. We found that the best χ^2 fit of the [O II] flux distribution skewed the fit of the faint-end slope—critical for our purposes here—to a steeper slope, $\alpha = -1.72$, than the data. To make a better fit of the faint-end slope, we used a one-sided Kolmogorov–Smirnov (K-S) test for goodness of fit to find the best-fitting slope. Consistent with what we had observed, this test ruled out this best χ^2 fit at the 97% confidence level, as described below.

The K-S test works with cumulative distributions. For this reason it is well suited to our application, since it is the cumulative source counts shown in Figure 4 that we want to model. The one-sided K-S test can be used to compare a model distribution, in this case an integrated Schechter LF, to observed data, here, cumulative [O II] counts; we used it to find the most probable faint-end slope and its allowable range. Both distributions were normalized to the interval 0.0–1.0 and the maximum fractional deviation and total count (2323 [O II] sources) was entered into an online K-S calculator[9] that returned the probability that the data were drawn from a distribution following the Schechter function. Since the two distributions are normalized, the only free parameter is the characteristic luminosity L^*. For each value of slope α we found the value of L^* that produces the minimum fractional deviation in the K-S test.

In Figure 7 we plot the probability that the [O II] data are drawn from a Schechter model of slope α, for the value of L^* that maximizes this probability. The best-fitting slope is $\alpha = -1.30$ and the equivalent of a 1σ interval is -1.05 to -1.50. What is in effect a 2σ rejection of the model occurs at $\alpha = -0.85$ and $\alpha = -1.70$. Figure 7 also shows the integrated deviations (in counts) for the four Schechter-function fits of the data, including the best χ^2 fit for the [O II] LF with faint-end slope of $\alpha = -1.72$. Though the residuals of this latter case are not large compared to Poisson errors, the S-wave shows a systematic error in the fit that accounts for the anomalously high value of α.

[9] http://www.ciphersbyritter.com/JAVASCRP/NORMCHIK.HTM#KolSmirof

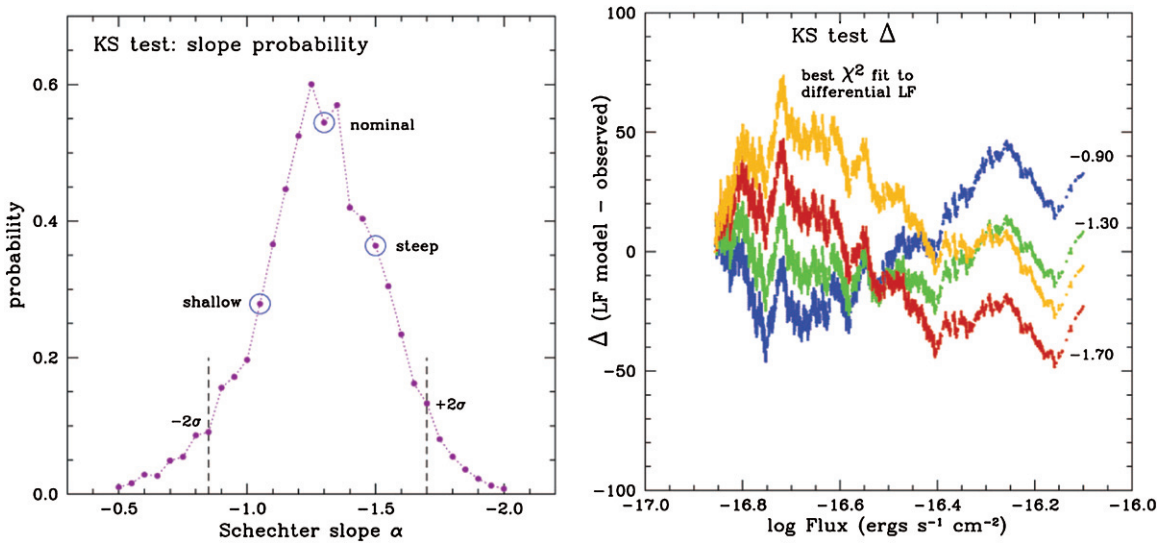

Figure 7. K-S test results of fitting Schechter functions to the [O II] counts. Left: the probability of fit for different values of the slope α and luminosity L^*. The two vertical dashed lines mark the slopes of $\alpha = -0.85$ and $\alpha = -1.70$, representing fits that are rejected at the ~95% level (2σ). Right: four examples of the fractional deviations Δ for best-fit Schechter functions and the [O II] counts. The larger the amplitude of the S-wave shape of the Δ distribution, the poorer the fit. The best fit, $\alpha = -1.30$, is nearly flat—well within the 1σ interval of "goodness of fit" of -1.05 to -1.50. The best χ^2 fit, shown in gold, shows a stronger S-wave that indicates rejection at the $P > 97\%$ level.

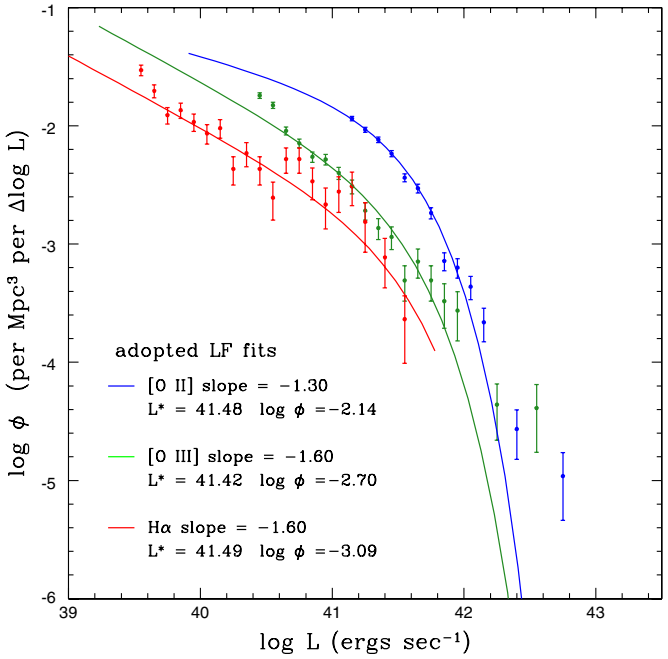

Figure 8. Differential LFs for sources in a 0.°7 radius circle surrounding the search field position. There are 2323 sources in the O II sample, 1491 O III sources, and 600 Hα sources within the 0.°7 circle that have been used for fitting luminosity functions (see the text). Slope values of -1.30, -1.60, and -1.60, respectively, have been used to extrapolate the expected number of foreground galaxies down to $F = 2.5 \times 10^{-18}$ erg s^{-1} cm^{-2}. The corresponding values of L^* in erg s^{-1} and log Φ in Mpc^{-3}(Δlog$L$)$^{-1}$ are recorded.

Choosing the K-S test to find the best-fitting slope makes sense because our application is insensitive to how well the [O II] distribution fits a Schechter function around L^*. If a Schechter function was known to be an excellent parameterization (as it is for broadband galaxy fluxes) for galaxy emission-line luminosities *uncorrected for extinction*, it could be argued that the faint-end extrapolation would be best made by giving as much weight to the curvature around L^* as to the power-law faint end. However, since the effects of extinction could subtly alter the form from a Schechter function, we believe that in this case a fit that gives more weight to the faint-end slope is preferred.

The adopted Schechter-function fits are compared to the binned differential counts in Figure 8. The values of the parameters (α, L^*, ϕ^*) we will use for the rest of this analysis are also given in the figure. In particular, the slopes we have derived are consistent with the values derived by other studies that made Schechter-function fits of foreground populations at these redshifts. For example, for [O II], [O III], and Hα slopes, respectively, Hippelein et al. (2003) find values of -1.45, -1.50, -1.35, and Ly et al. (2007) find values of -1.15, -1.22, -1.70. For the COSMOS Survey itself, Takahashi et al. (2007) report an [O II] slope of -1.41 and Shioya et al. (2008) report an Hα slope of -1.35.

5.4. Subtracting Extrapolated Foreground Populations to Measure the LAE Luminosity Function

We have used these LFs and their extrapolations 2×10^{-18} erg s^{-1} $< F < 10^{-17}$ erg s^{-1} cm^{-2} to predict foreground contamination down to the limit of our survey. In Figure 9 we compare the counts of our LAE search (shown in Figure 4) to the observed COSMOS foreground counts (blue, green, and red lines for [O II], [O III], and Hα, respectively) and the Schechter-function fits to these counts (solid magenta lines, then dotted for the extrapolation). Though we have used all the data within the 0.°70 circle—2323 [O II], 1491 [O III], and 600 Hα sources—to fit the LFs, we normalize to the counts for these foregrounds in the IMACS search field, 358, 201, and 81, respectively, for a total of 640. The summed result is the dashed green line marked "COSMOS" in Figure 9. This summed COSMOS foreground is a very good fit to the "Em+C" counts of our LAE search—the red line, down to $F = 10^{-17}$ erg s^{-1} cm^{-2}. Fainter than this, the *extrapolated* COSMOS foreground falls between the certain foreground (red) and total observed (blue), suggesting that while some of the SEL sources are foreground, many are plausibly identified as LAEs. Using these nominal slopes, then, typical of those measured for comparable galaxy populations at $z \lesssim 1$,

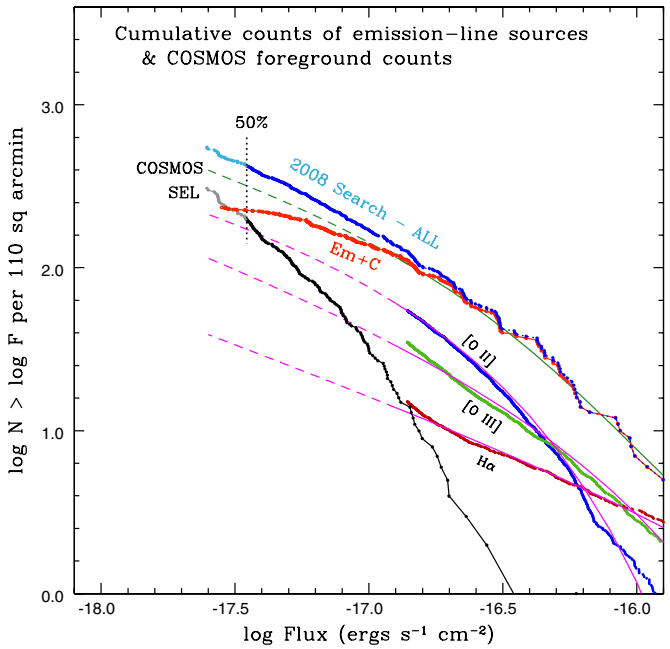

Figure 9. Same as Figure 4, but including cumulative counts of Hα, [O III], and [O II] foregrounds from the COSMOS Survey catalog of Takahashi et al. (2007), with fits to Schechter functions made by us for extrapolation fainter than $F = 10^{-17}$ erg s^{-1} cm^{-2}. As before, the "ALL" line is the sum of SEL and Em+C sources. (The adopted incompleteness correction described in Section 4 has been applied. The vertical bar marks the 50% incompleteness at $F = 3.5 \times 10^{-18}$ erg s^{-1} cm^{-2}: at this point the cumulative "ALL" counts are greater by 7.0% than for an uncorrected distribution.) The "COSMOS" line is the sum of these three expected foreground interlopers, as explained in the text. Since the "ALL" line of our 2008 survey is a sum of foreground sources and LAEs at $z = 5.7$, if the extrapolated foreground of the COSMOS data accurately represents all foreground objects, then its difference from the "ALL" line of our search should be due entirely to LAEs.

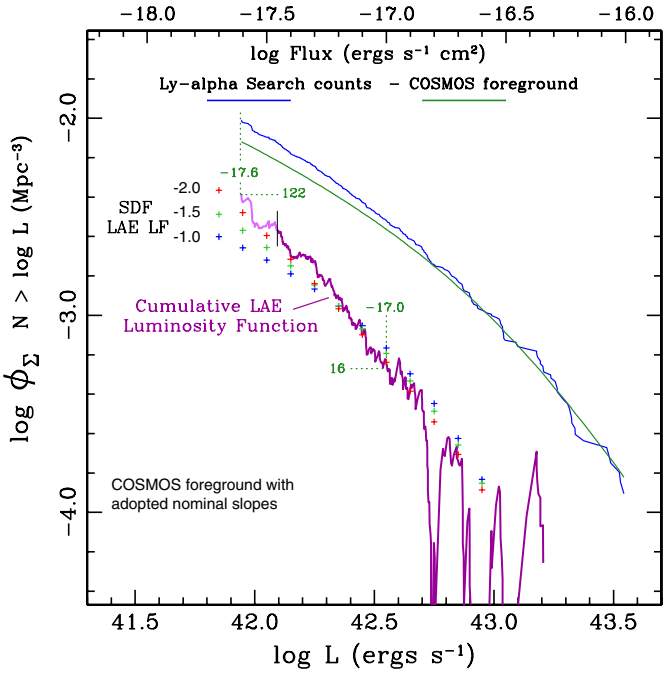

Figure 10. Cumulative LF for Lyα emitters (purple line) derived from subtraction from the search "ALL" counts (blue line) of Schechter-function fits to COSMOS foreground counts (green line). The magenta line is the foreground-subtracted cumulative LF derived using the nominal Schechter LF slopes of $\alpha = -1.30$, -1.60, and -1.60 ([O II], [O III], and Hα), as described in the text. As in the previous figures, the data are cumulative rather than binned: this accounts for the wild excursions at the bright end of the LF, points where the predicted foreground exceeds the few counts of our comparatively small-volume survey. The point of 50% completeness is marked with a short vertical line and a lighter purple to our survey limit. Also shown are SDF LF function extrapolations for the LAE emitters found in narrow-band searches by Shimasaku et al. (2006). Our derived LF for LAEs rises in accordance with the *predicted* SDF model for a differential faint-end slope of $\alpha = -2.0$. The cumulative counts in our survey area increase from $n \approx 16$ for $\log L$ (erg s^{-1}) > 42.55 to $n \approx 122$ at the limit of our survey, $\log L$ (erg s^{-1}) $= 41.95$.

leads to the conclusion that the steep slope of SEL sources is due in part to an increasing fraction of LAEs.

We quantify this in Figure 10, which shows the cumulative LF of LAEs obtained by subtracting the extrapolated COSMOS foreground. The upper blue and green lines (identical to those in Figure 9) correspond to the total observed counts (corrected for incompleteness) and the predicted foreground counts from fits to the COSMOS NB816 data. The difference—"observed" minus "foreground"—is shown as the magenta line and compared to the *extrapolation* of the fits to the LF for LAEs in the SDF (Shimasaku et al. 2006).

We find that normalizing the foreground to the total $n = 640$ sources in the full $1/2^\circ$ field of IMACS results in a cumulative LF with 16 LAEs down to $F = 10^{-17}$ erg s^{-1} cm^{-2}, about 6% higher than the number found by integrating the LAE LF of the larger SDF survey (Shimasaku et al. 2006), scaled to the ∼5 times smaller volume of our survey of 30,366 Mpc^3. However, this excellent agreement must be in largely fortuitous since the SDF LF includes modeling for incompleteness and survey boundaries—not attempted here—that make differences at the 10%–20% level. Our normalization has additional uncertainty of at least 10% due to its sensitivity to the amount of subtracted foreground, which we do not know better than a few percent due to Poisson fluctuations, and also because we do not as yet have independent measurements of the foreground in the 15h search field. While the agreement in the space density of LAEs brighter than $F = 10^{-17}$ erg s^{-1} cm^{-2} gives us confidence in our foreground-subtraction analysis, we adopt the SDF normalization and conclude that the agreement of our LAE density with that of SDF is, if anything, better than expected and thus provides no new information on the LAE volume density.

Comparing the slope of putative LAE sources fainter than $F = 10^{-17}$ erg s^{-1} cm^{-2} with the SDF *predicted* LF over this range, our measured LF follows the steepest of the SDF models with slope $\alpha = -2.0$, as Figure 10 shows. Using this nominal model of the foregrounds, the cumulative number of LAEs rises from 16 at $F = 10^{-17.0}$ erg s^{-1} cm^{-2} to $n \approx 122$ at $F = 10^{-17.6}$ (2.5×10^{-18}) erg s^{-1} cm^{-2}. The steep rise in LAEs found by statistically subtracting the foreground contamination produces a result that is not greatly different from the SEL sample (see Figure 9), which means that a substantial fraction of the SEL-only sources (compared to a much smaller fraction of *all* emission-line sources) are predicted to be LAEs. The steep rise attributed to LAEs is also consistent with the result of the cross-correlation analysis in Section 5.2. Although only circumstantial as opposed to the direct evidence of high-resolution spectroscopy, the agreement in result for the two fully independent analyses of (1) LAE LF by background-subtraction and (2) angular correlation function of foreground and candidate LAEs, provides some confidence that approximately half of the faint SEL sources we have found are LAEs. This is the main conclusion of this paper.

The critical reader will remember that the result of the cross-correlation analysis of Section 5.2 implied that at most about half of the faint LAE candidates are members of the

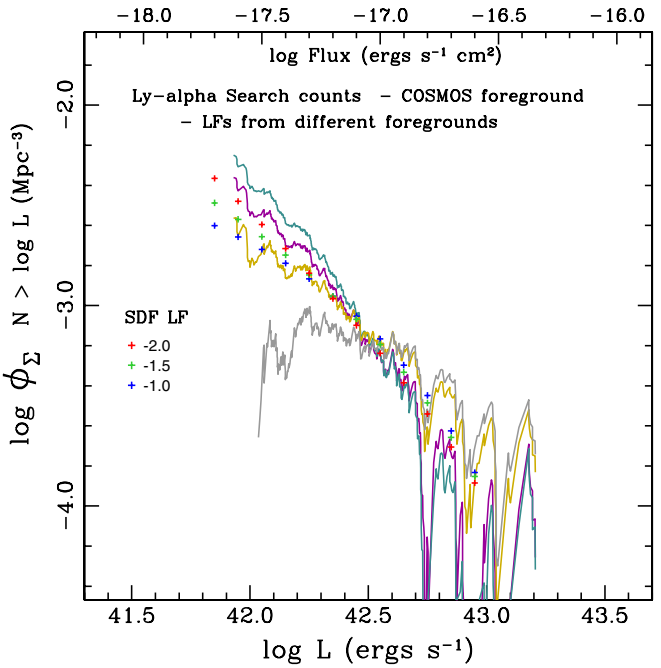

Figure 11. Same as Figure 10, but for shallower and steeper Schechter-function slopes for the foreground populations. The magenta line is the LF derived for the nominal slopes shown in Figure 10, which approximately matches the extrapolated Subaru Deep Field LAE counts with a slope $\alpha_{\rm LAE} \approx -2.0$. The LF above (turquoise) has the nominal [O III] and Hα slopes but the -1σ shallower [O II] slope of -1.05 (see Figure 8), which leads to a steeper LAE LF with $\alpha_{\rm LAE} \approx -2.5$. Steeper slopes of the nominal foreground fits, $-$ 1.50, -1.65, and -1.65 ([O II], [O III], Hα (see the text) produce the shallower LAE LF (gold line) with $\alpha_{\rm LAE} \approx -1.3$. Within this range of foreground fits the basic result of a rising LAE LF is maintained. However, steepening the foreground population slopes further to -1.70, -1.70, and -1.70 makes the rising LAE LF disappear (gray line), in fact, there are no added LAEs fainter than $F = 10^{-17}$ erg s^{-1} cm^{-2}. As explained in the text, there are reasons to be dubious of this model, including its inconsistency with the brighter LAE LF of SDF, the angular correlation results of Section 5.2, and the "fine tuning" it requires.

foreground population. The foreground-subtraction analyses suggest that at $F = 10^{-17}$ erg s^{-1} cm^{-2} only about 15% of all emission-line sources are predicted to be LAEs, whereas this fraction rises to ~50% at the limit of our survey, $F = 10^{-17.6}$ (2.5×10^{-18}) erg s^{-1} cm^{-2}. Thus, the two independent approaches yield the same approximate result, though there is still considerable latitude in both estimates.

5.5. Placing Limits on the LAE Luminosity Function

The uncertainty to be attached to the LF shown in Figure 10 is not governed by the counts of sources. Much larger changes in the derived LAE LF come from the uncertainty in the level of foreground contamination. First, there is the statistical uncertainty in fitting the COSMOS foregrounds counts with Schechter functions. As described in Section 5.2, there are a range of slopes (with corresponding values of L^*) that can fit the data; in Section 5.4 we used only the "best-fit" values. Flatter slopes for the foreground LFs will increase the amplitude and steepness of the LAE LF, while steeper slopes for the foreground will do the opposite. The foreground with the most leverage is [O II], although we steepen somewhat the slopes of [O III] and Hα as well. The turquoise line in Figure 11 shows the result of adopting the -1σ fit (see Figure 8) of the Schechter LF for [O II] $\alpha = -1.05$: even if the [O III] and Hα slopes are left at their steeper "nominal" values, the flatter [O II] LF produces an even stronger climb in the LAE LF, $\alpha_{\rm LAE} \approx -2.5$, compared with the nominal result of Figure 10 (the magenta line in Figure 11). Conversely, a steeper [O II] slope $\alpha = -1.50$ ($+1\sigma$) with [O III] and Hα slopes of $\alpha = -1.65$ produces a flatter LAE LF (gold line), but it is still prominent with $\alpha_{\rm LAE} \approx -1.3$. Therefore, a rising LAE LF, while quantitatively sensitive to the amount of foreground contamination, holds over a substantial and reasonable range of foreground contamination.

In addition to these statistical errors to the fits in the COSMOS foreground counts, we must consider systematic errors in determining the foreground that can influence the LAE LF derived by this technique. We have in fact used only the foregrounds from the COSMOS Survey, but we have applied this foreground to both the 10h (COSMOS) and 15h (LCIRS) fields for which we have produced counts of emission-line sources with and without continuum. Cosmic variance is expected and this could have a substantial effect on our LAE LF. For example, Ly et al. (2007) fit Schechter functions to emission-line source counts uncorrected for extinction in the SDF. Using photometric selection techniques different from the COSMOS study we use here, Ly et al. obtain an almost identical normalization of counts at $F = 10^{-17}$ erg s^{-1} cm^{-2} compared to COSMOS, and respective ratios of Hα, O III, and O II of 13%, 23%, and 64%, compared to 13%, 32%, and 55% for the COSMOS foregrounds—an inconsequential difference. However, despite very similar L^* values for these three LFs, the much flatter slopes of the LFs derived by Ly et al., $\alpha = -1.15$ for O II and -1.22 for [O III], result in a 15% lower foreground at the limit of our study, $F = 10^{-17.6}$ erg s^{-1} cm^{-2}, and predict an even larger population of LAEs than our nominal result. Accordingly, there are also considerably higher counts for the bright end of the LF compared to COSMOS, which leads to a considerable oversubtraction from all our own MNS counts of bright sources.

The Ly et al. example again points to faint-end slopes as the key issue. The bright end of each foreground LF, in contrast, is sensitive to the normalization and exponential cutoff of the Schechter LF and not well constrained by the comparatively small volume of our survey. For this reason, although we have not needed to renormalize the COSMOS-derived foregrounds before subtracting from our MNS counts, we would have considered it acceptable to do so and to concentrate our attention on the faint-end slopes, where the case for a steeply rising LAE LF is made or broken. Because they are well below the L^* values of these LFs, our extrapolations of LF fits to the measured COSMOS counts are essentially power laws: our result does not depend on the *shape* of the LF, either theoretically or as measured.

Comparing our own MNS counts in the two fields, we find evidence for both variation and consistency. Including the incompleteness correction in both, our total counts of all emission-line sources are very close at 276 in the 10h field compared to 258 in the 15h field. However, the bright ends of the LF are strikingly different: 19 of the 20 sources brighter than $F > 5 \times 10^{-17}$ erg s^{-1} cm^{-2} are from the 10h field. Approximately two thirds of these are identified to be Hα using our short spectra (as is predicted from the COSMOS LFs shown in Figure 9), however, it appears that large-scale structure has caused Hα to be over- and underrepresented in the 10h and 15 h fields.[10] Basically, then, the faint end (power-law) slopes of the LF fits to the foreground populations dominate the

[10] From these semi-reliable line identifications from the MNS survey data, for which [N II] λ6548, λ6583 and [O III] λ4959 are sometimes apparent, we determined ratios of 53%, 31%, and 16% for [O II], [O III], and Hα, respectively, in good agreement with the proportions determined in COSMOS.

uncertainty in our result of a steeply rising LAE LF, whether this comes from statistical errors in fitting the COSMOS counts or in uncertainties that arise from cosmic variance that projects different proportions of the three main foregrounds into our two fields.

Focusing on faint-end slopes, then, we find that a complete loss of the LAE signal for our survey requires pushing the slopes of all three foregrounds to $\alpha = -1.70$. For the [O II] LF this is a $+2\sigma$ excursion from the best fit of the COSMOS data. Such steep slopes for the foreground populations can account for all of the observed SEL plus Em+C sources. As seen in Figure 11, the resulting cumulative LF (the gray line) is flat, which means that *no* LAEs are added fainter than $F = 10^{-17}$ erg s^{-1} cm^{-2}. We find this possibility unlikely for three reasons. (1) It is inconsistent with the LAE LF found in the SDF, which rises far faster up to $F = 10^{-17}$ erg s^{-1} cm^{-2} and shows no sign of turning over at that point. (2) It is inconsistent with the lack of correlation between these faint sources and the COSMOS foreground (Section 5.2). (3) It requires "fine tuning" the slopes of the foreground population—a wide range of slopes, $-0.85 < \alpha < 1.50$ for both [O II] and [O III] (encompassing the values found by all other studies), lead to a rising LAE LF, but only a narrow range $1.60 < \alpha < 1.70$ leads away from this conclusion. For these reasons we consider a rising LAE LF to be the most probable interpretation of our MNS survey data, and the one we favor.

To summarize, we have used the COSMOS foreground counts to subtract from our full ensemble of emission-line sources and found a steeply rising LAE LF that is significant at the $\sim 2\sigma$ level, where this is set by the statistical uncertainty in the foreground contamination rather than by the number of faint emission-line sources we have observed. Systematic errors will play a significant role only if they affect the faint-end slopes of the LFs for foreground sources. Within broad limits of the faint-end slopes of the foreground LFs, the result of a rising LAE LF is secure. Nevertheless, this exercise has confirmed that measuring the LAE LF faint slope to $\pm 10\%$ is probably not possible with this method alone, due to the sensitivity of a rising LAE LF to the foreground subtraction. This highlights again the importance of spectroscopic confirmation for these faint candidate LAEs. While difficult, this can be done with existing facilities and is ongoing.

6. DISCUSSION

Early galaxies are central to the hierarchical assembly of present-day galaxies, the dispersal of heavy elements, and the reionization of intergalactic hydrogen. The number density of low mass galaxies is arguably the most important unknown in each of these chapters of cosmic history.

The 2008 MNS survey we present in this paper is unprecedented in its combination of depth and volume. The faintest $z \approx 5.7$ Lyα emission lines found in the survey have a line luminosity of $L(\mathrm{Ly}\alpha) = 7.0 \times 10^{41}$ erg s^{-1}, which is nearly five times deeper than narrow-band imaging surveys for LAEs. The only known sources of comparable luminosity at $z \sim 5.7$ have either been found in the UDF and UDF Parallels (e.g., Bouwens et al. 2006; Stanway et al. 2007), behind foreground clusters (Ellis et al. 2001; Santos et al. 2004), or in the 3.3 arcmin^2 "Ultra-deep" serendipitous VIMOS Deep Survey (Cassata et al. 2011). Our MNS survey covers a far greater volume than these studies. The measured FWHM filter bandpass of (8115–8249 Å) of our MNS survey samples Lyα emission over a redshift interval of $\Delta z = 0.11$ at $z = 5.75$, producing an effective survey volume of 1.52×10^4 Mpc^3 per mask, two-orders-of-magnitude larger than the HUDF for an equivalent redshift slice. Moreover, as a result of the layout of our slit mask, our survey sparsely samples an area of sky 10 times larger than the solid angle subtended by the slits. For the two-field survey, then, our total survey volume of 3.04×10^4 Mpc^3 is actually drawn from a 3×10^5 Mpc^3 volume, substantially reducing the effect of cosmic variance.

The area of the slits used to probe gravitational lens caustics in clusters of galaxies is also tiny compared to our MNS mask, and magnification by the lens further reduces the survey volume. For example, Santos et al. (2004) present survey volumes up to 10^4 Mpc^3 over the a broad redshift range corresponding to $\Delta z \approx 2$. In contrast to this pencil-beam footprint, our survey volume is more nearly cubical, making our MNS survey much better suited to constraining the faint-end slope of the LAE LF.

6.1. The Connection of Low-luminosity LAEs to Galaxies like the Milky Way

While mindful of the critical importance of spectroscopic confirmation of our LAE candidates, we adopt for purpose of the following discussion the nominal LAE LF shown in Figure 10 based on the most probable foreground subtraction. Our MNS survey finds a surface density $N \gtrsim 1$ LAE candidate per square arcminute, for log $L(\mathrm{Ly}\alpha)$ (erg s^{-1}) > 41.95. With a redshift interval of $\Delta z = 0.11$, this amounts to a space density of approximately 4×10^{-3} Mpc^{-3}, comparable to that of today's L^* galaxies. For example, Loveday et al. (1992) and Marzke et al. (1994) find Schechter-function values $\phi^* \approx (5\text{–}10) \times 10^{-3}$ Mpc^{-3} for the local galaxy population. Integrating the LF with the slope $\alpha = -1.0$ found by these studies, the space density of galaxies brighter than about $L^*/3$ in the local universe matches the comoving space density of our candidate LAEs. Stated another way, we have found three or four sites of active star formation per future L^* galaxy.

Today's L^* galaxies have typical halo masses of $M = (1\text{–}2) \times 10^{11}\, M_\odot$. From analyses of merger trees in ΛCDM simulations of the growth of structure, Stewart et al. (2008) find that the halo mass of such objects at $z \sim 6$ is an order-of-magnitude smaller, $M = (1\text{–}2) \times 10^{10}\, M_\odot$, and that these will grow into today's typical galaxies principally through accretion of smaller halos of ∼10% of their mass. Interestingly, a halo mass of $\sim 10^{10}\, M_\odot$ can also be inferred for LAEs at the density found by our survey by comparing to the LAE study by Ouchi et al. (2010), who derive a halo mass of $M = 10^{10}\text{–}10^{11}\, M_\odot$ from the clustering strength of a large sample of brighter LAEs, $L > L^*$. Although our sample is too small, and not well constructed to measure correlation statistics, it is reasonable to assign halo masses an order-of-magnitude smaller to the much less luminous LAEs of our study, $\sim 10^9\text{–}10^{10}\, M_\odot$. This in turn suggests a stellar mass of $\sim 10^8\text{–}10^9\, M_\odot$.

The fraction of all galaxies that are detectable as LAEs at this redshift remains uncertain, so sampling issues are another important consideration in this comparison. Our survey has only recovered galaxies with vigorous star formation and exhibiting Lyα emission. These LAEs could be short-lived starbursts, so we might only be detecting a fraction of such galaxies at this mass. Ouchi et al. estimate a ∼1% duty cycle, but Stark et al. (2011) argue for a value much closer to unity, as perhaps does our own finding of a steep faint-end slope of $\alpha \sim -2.0$ for the LAE LF, if this is a manifestation of Lyα luminosity following halo mass. Whether large or small, the correction for duty cycle

will surely increase the luminosity density our MNS survey implies.

In addition, we may be finding only the fraction of active objects to which our view is not obscured by dust. Although there is some reason to expect that this is becoming less of a factor for higher redshift, lower-luminosity systems (Bouwens et al. 2009), here again we can be sure of the sign of the effect, and in this case the steepness of faint-end slope does not limit this effect to being a small one. In summary, we can be fairly certain that our survey identifies only a fraction of the galaxies of this dynamic period of star formation and assembly, implying a higher space density of galaxies for a population that, according to our result, already outnumber future L^* galaxies by a factor of 3–4.

By number density arguments, then, we can be confident that faint LAEs are not components of the most massive objects at $z \sim 6$, but more likely progenitors of today's L^* galaxies. However, it is less clear whether these LAEs are in fact part of the main structure of such a galaxy (e.g., the early halo or bulge) or instead some accreted satellite or lower mass dwarf system that is destined to become part of the L^* galaxy. Significant advances in understanding what role these systems play are beyond present observational capabilities. Eventually, however, with measurements of stellar and dynamical masses, and large enough samples for an accurate correlation function statistics, the nature of this basic, populous component at a crucial epoch of galaxy growth will become clear.

6.2. The Properties of Galaxy Building Blocks

While Lyα luminosity is admittedly a poor indicator of star formation rate, due to radiative transfer effects in galaxies, we note that the standard Case B conversion gives star formation rates as low as SFR $= 0.84 f_{\rm Lya}^{-1}(F(\ {\rm erg\ s^{-1}\ cm^{-2}})/2.5 \times 10^{-18})\ M_\odot\ {\rm yr}^{-1}$ for the faintest objects in our new sample of LAEs. If star formation lasts for at least a dynamical timescale, $\tau \gtrsim 5.0 \times 10^7$yr, and half the Ly$\alpha$ photons escape, $f_{\rm Ly\alpha} \approx 0.5$, then these galaxies must have built up stellar masses of at least $10^8\ M_\odot$, consistent with what we derived above based on estimates of halo masses of $\sim 10^9$–$10^{10}\ M_\odot$.

It is interesting to compare this mass scale to some of the earliest building blocks of present-day galaxies. The surviving Milky Way satellites and globular clusters (GCs) may be the oldest intact stellar systems that formed near the end of the reionization era. The characteristic stellar mass scale of GCs today is $1.4 \times 10^5\ M_\odot$ (Harris 1991). Even if the initial masses of GCs are, as estimated, at least 8–25 times larger (Schaerer & Charbonnel 2011), it still follows that the faint LAEs probably contain more stellar mass than early GCs. By this argument, the faint LAEs discussed hear probably represent either the main body of a proto-Milky-Way galaxy or its satellite galaxies.

We can also consider the fate of the heavy elements synthesized by galaxies near the end of the reionization era. From the distribution of intervening metal-line systems at redshift $z \sim 3$, we know that the metals ejected by galaxies present a high clustering bias. Although the LBGs studied by Adelberger et al. (2005) are similarly clustered and have been shown to harbor strong outflows (Steidel et al. 2011), their stellar populations are not generally old enough to have spread metals over the large enriched regions recently identified using tomographic studies of intervening metal-line systems (Martin et al. 2010). These authors argue that lower mass galaxies at higher redshift dominate the dispersal of heavy elements and show that winds from redshift $z \sim 6$ galaxies with halo masses of $(0.5\text{–}2.0) \times 10^{10}\ M_\odot$ would have left very large bubbles of metals around LBGs at $z \sim 3$. Therefore, by parameters of space density and mass, our faint LAE sample appears to be a good match to this hypothesized galaxy population. We therefore expect strong gaseous outflows from these objects, a prediction that can be tested with additional spectroscopy. Since these enriched bubbles may persist long after the star formation in these galaxies, their redshift density could eventually constrain the duty-cycle of low-luminosity LAEs.

6.3. Faint LAEs, the Lyman Continuum, and Reionization at $z \sim 6$

The production of Lyman-continuum photons by galaxies at $z \sim 6$ has been of particular interest since the discovery that intergalactic hydrogen is almost entirely ionized by this time (Becker et al. 2001; Fan et al. 2002, 2006). *Wilkinson Microwave Anisotropy Probe* measurements point to a significant ionization fraction by around $z \sim 11$ (Spergel et al. 2007; Page et al. 2007), but the recombination time of intergalactic protons is short compared with the time between $6 < z < 11$. An ionized IGM at $z = 6$, therefore, requires a critical density of star formation or another, as yet unidentified, source of Lyman-continuum radiation.

For many years it has been recognized that low-luminosity galaxies at $z \gtrsim 6$ played an important role in the reionization of the universe (Lehnert & Bremer 2003; Stanway et al. 2003; Bouwens et al. 2007). These studies found many galaxies at $5 < z < 7$ that are fainter than the knee in the luminosity, but the implied star formation density of the detected galaxies falls well below the critical level required to maintain reionization. Thus, even more sensitive surveys are required to identify this lower-luminosity population of galaxies that maintains reionization. Our MNS survey has taken a significant step in finding faint Lyα emission from galaxies whose continuum radiation could be undetectable with any available facility.

With this as background, we revisit the question explored in Martin08 of the possible contribution of faint LAEs to the reionization budget of the IGM at $z \sim 6$. As discussed in Martin08, the critical star formation rate density at $z \sim 6$ required to keep the intergalactic hydrogen ionized depends on the physical properties of galaxies and the IGM. The production rate of Lyman-continuum photons, the fraction of Lyman-continuum photons that escape from galaxies ($f_{\rm LyC}$), and the clumpiness of the IGM (C) may all evolve significantly over the first few billion years of galaxy formation. Martin08 grouped these dependencies into a single parameter $\zeta \equiv C_6(1 - 0.1 f_{\rm LyC,0.1}) f_{\rm Ly\alpha,0.5}/f_{\rm LyC,0.1}$; $\zeta \sim 1$ corresponds to the current best guesses for these parameters. Values of $\zeta < 0.2$, or $\zeta > 5.0$, would require significant modifications to our current understanding of these physical properties.[11] In addition, the intergalactic gas temperature of 10^4 K we assume is also conservative. Higher temperatures would lower the recombination rate and thereby reduce the number of Lyman-continuum photons required for reionization.

Martin08 used the LAE LF parameters L^*, ϕ^*, and α to estimate the number of ionizing photons. The production of Lyman-continuum radiation by stars is quite uncertain for any individual LAE. For the population as a whole, however, under

[11] Here, we have parameterized $C_6 = C/6$, and $f_{\rm LyC,0.1} = f_{\rm LyC}/0.1$. Likewise, the escape fraction of Lyα photons is given as $f_{\rm Ly\alpha,0.5} = f_{\rm Ly\alpha}/0.5$. The "best-guess" values of these renormalizations are discussed in more detail in Martin08.

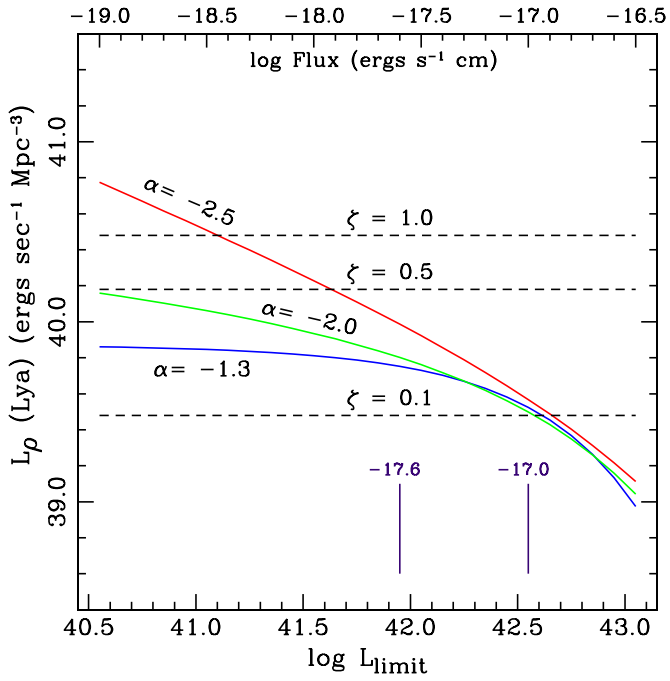

Figure 12. Level of luminosity density required for maintaining reionization at $z \sim 5.7$ with a population of faint LAEs. The green, blue, and red curves show the integrated luminosity density for the three values of faint-end slope α −1.3, −2.0, and −2.5, respectively, that characterize the "best fit" and $\pm 1\sigma$ bounds of our LAE LF result. For slopes $\alpha < -2.0$ there is substantial progress toward reaching critical flux density, $\zeta = 1$, from our prior limit (Martin08) of the LAE LF, log L (erg s^{-1}) $\sim$ 42.55, to the lower-luminosity limit of the MNS survey. By log L (erg s^{-1}) $\sim$ 41.95 about 20% if the critical flux density $\zeta = 1.0$ has been reached with the $\alpha = -2.0$ slope, or about 40%, if the Lyman-continuum escape fraction is as high as 20%, or *all*, for an escape fraction of about 50%—not impossible for these low-luminosity, high-z LAEs. Extrapolation to fainter limits, and/or a steeper slope of $\alpha = -2.5$, further increase the likelihood that LAEs alone can provide the critical flux density to complete reionization at $z \sim 6$.

the standard Case B recombination assumption, a galactic nebula produces two Lyα photons for every three Lyman-continuum photons absorbed by the galaxy; we assume that, on average, one of the two Lyα photons escapes from the galaxy, i.e., $f_{\mathrm{Ly}\alpha} = 0.5$. We adopt the "best-fit" faint-end slope of $\alpha = -2.0$ and the $\pm 1\sigma$ bounds, $-1.3 > \alpha > -2.5$, that come from varying the foreground contamination (see Section 5.3) in our new MNS survey. Shimasaku et al. (2006) give fits to L^* and ϕ^* for slopes $\alpha = -1.0, -1.5, -2.0$. We interpolated, and extrapolated, respectively, to find appropriate [L^*, Φ^*] values for the $\alpha = -1.3$ and $\alpha = -2.5$ limits. For the slopes of $\alpha = -1.3, -2.0, -2.5$ the adopted values are determined as log L^* (erg s^{-1}) = 42.81, 43.20, 43.63 and log ϕ (Mpc^{-3}) = −3.05, −3.80, −4.71. The three curves in Figure 12 show the integration of flux density to decreasing luminosity limits and compares this to the value ζ described above that represents the required luminosity density to keep the IGM ionized.

A firmer constraint on the LAE LF allows us to better estimate the fraction of the critical ionizing flux that faint LAEs contribute to maintaining ionization at $z \sim 5.7$. Our new data indicate a steep faint-end slope $\alpha \sim -2$ (see Figure 10), so for purposes of our discussion here, we revisit only the luminosity-density calculation shown in Figure 13 of Martin08 for $\alpha = -2.0$. That diagram showed a strong covariance of L^* and Φ^* that produced a banana-shaped region of values that were compatible with the few data of that analysis. However, if we use our new MNS results to constrain the faint-end slope and adopt the [L^*, Φ^*] values obtained by Shimasaku et al. (2006) for Schechter-function fits for the SDF data, the analysis is more straightforward. We recognize that both the faint-end slope from this work and the L^* and Φ^* values from the SDF survey continue to have significant uncertainties, so our analysis here is only for the best values available.

In Figure 12 we plot the integrated luminosity density, $\mathcal{L}_\rho$, for the LFs with faint-end slopes $\alpha = -1.3, -2.0, -2.5$ shown in Figure 11. Summing the Lyα luminosity down to log L (erg s^{-1}) = 42.55 falls short by an order of magnitude of the $\zeta = 1$ case. Our new data are relatively complete down to log L (erg s^{-1}) = 41.95. With $\alpha = -2.0$ and the Shimasaku et al. normalization, our new population of LAEs comes up a factor of five short for maintaining the ionization of the IGM at $z = 5.7$. However, looking at this result another way, if the escape fraction of Lyman-continuum photons from these galaxies were 50% ($\zeta = 0.2$) instead of the assumed value of 10%, then the population that we detected can fully ionize the IGM.

For purposes of further discussion we assume that the LAE LF slopes we derive hold to much fainter luminosities. For example, our best-fit value of $\alpha = -2.0$ for the LAE LF needs to hold to a luminosity 28 times fainter—to log L (erg s^{-1}) = 40.5—to reach critical flux density for an escape fraction of 20%, $\zeta = 0.5$. With the steeper faint-end slope of $\alpha = -2.5$—consistent with our survey result at the 1σ level—our counts are already sufficiently deep to reach critical flux density $\zeta = 0.5$, and even $\zeta = 1.0$ requires only a factor of $\sim$7 extension to fainter LAEs, to log L (erg s^{-1}) = 41.1.

If the rising LF for faint LAEs we have derived is correct, an important step has been taken toward finding the galaxies that could maintain the ionization of the IGM at $z = 5.7$. At $z \sim 6$, however, direct measurement of the Lyman-continuum escape fraction is precluded due to the attenuation of the Lyman continuum by intergalactic hydrogen. Proof that the faint LAE galaxies can maintain the ionization of the IGM will rest on indirect arguments about their Lyman-continuum escape fraction. One approach is to extrapolate from direct measurements at lower redshift. Another approach is to model the nebular emission.

In contrast to the normal situation, where the far-UV continuum is dominated by stellar continuum, the nebular continuum is several times brighter than the stellar continuum for extremely young star clusters (see Figure 5 of Schaerer 2002). Even for less extreme conditions, the nebular continuum makes a significant contribution to the far-UV luminosity. The hydrogen two-photon continuum makes the galaxy appear redder than its intrinsic stellar spectral energy distribution. Figure 3 of Bouwens et al. (2010) illustrates this effect as a function of stellar age and suggests that less extreme nebular emission still impacts the continuum slope. Most significantly, nebular emission prevents the continuum slope from getting bluer than about $\beta \sim -2.5$.[12] This limit is relevant because bluer values of β have been reported in low-luminosity galaxies at high redshift (Bouwens et al. 2009, 2010). The escape of Lyman-continuum photons, by definition, reduces the nebular emission and offers one plausible explanation of extremely blue far-UV color. In summary, if it turns out that our faint LAEs exhibit very blue far-UV continuum slopes, e.g., $\beta < -2.5$, this would be an argument that the escape fraction of Lyman-continuum photons in these galaxies is significant.

[12] The far-ultraviolet continuum slope is defined by $f_\lambda \propto \lambda^\beta$ or $f_\nu \propto \nu^{-(\beta+2)}$ (Meurer et al. 1999).

7. CONCLUSION

We carried out a blind, wide-field emission-line survey, detected line fluxes as low as 2×10^{-18} erg s^{-1} cm^{-2}, and discovered what appears to be a steep rise in the number counts of emission-line galaxies. Extrapolation of the number counts for well-measured, foreground populations suggests that $z = 5.7$ LAEs, reaching $L = 7 \times 10^{41}$ erg s^{-1}, comprise a substantial fraction of the faint counts of the MNS survey sample, and that the implied faint-end slope of the LAE LF is close to $\alpha = -2.0$. The detected galaxies would then be a major contributor to the sources of Lyman continuum that completed the reionization of the universe at $z \sim 6$. Because of their high number density (several times that of today's L^* galaxies, and even higher, if such factors as duty cycle and preferred viewing angles are important), these faint LAEs are likely building blocks of today's common galaxies.

It should be possible to estimate the escape fraction of Lyman-continuum photons from measurements of the UV-continuum slope of these faint LAEs. Extremely blue values of the continuum slope β in the rest-frame, far-UV between Lyα and roughly 2000 Å would provide evidence for suppressed two-photon continuum emission and, indirectly, indicate a high escape fractions of Lyman-continuum photons. Such measurements are already possible by using WFC3 on the *HST* to obtain very deep infrared photometry of these fields. Measurements of this type with greater depth and quality will become routine with the *James Webb Space Telescope*.

The authors thank the referee for a careful reading of the manuscript and many useful suggestions. They also acknowledge important help and discussions by colleagues Peter Capak, T. J. Cox, Janice Lee, and Chun Ly, and comments from Kristian Finlator and Moire Prescott on the presubmission draft. Dressler recognizes the critical contribution to this work by the National Science Foundation through a 2006 *TSIP* grant, administered by AURA/NOAO, that supported construction of a new mosaic CCD camera and made these observations possible. C.L.M. acknowledges support for this project through the David and Lucile Packard Foundation. This research has made use of the NASA/IPAC Infrared Science Archive, which is operated by the Jet Propulsion Laboratory, California Institute of Technology, under contract with the National Aeronautics and Space Administration.

REFERENCES

Adelberger, K. L., Steidel, C. C., Pettini, M., et al. 2005, ApJ, 619, 697
Becker, R. H., Fan, X., White, R. L., et al. 2001, AJ, 122, 2850
Bouwens, R. J., Illingworth, G. D., Blakeslee, J. P., & Franx, M. 2006, ApJ, 653, 53
Bouwens, R. J., Illingworth, G. D., Franx, M., & Ford, H. 2007, ApJ, 670, 928
Bouwens, R. J., Illingworth, G. D., Franx, M., et al. 2009, ApJ, 705, 936
Bouwens, R. J., Illingworth, G. D., Oesch, P. A., et al. 2010, ApJ, 708, L69
Bouwens, R. J., Illingworth, G. D., Thompson, R. I., et al. 2004, ApJ, 606, L25
Bunker, A. J., Stanway, E. R., Ellis, R. S., & McMahon, R. G. 2004, MNRAS, 355, 374
Cassata, P., Le Fvre, O., Garilli, B., et al. 2011, A&A, 525, A143
Cowie, L. L., Barger, A. J., & Trouille, L. 2009, ApJ, 692, 1476
Cowie, L. L., & Hu, E. M. 1998, AJ, 115, 1319
Crampton, D., & Lilly, S. 1999, in ASP Conf. Ser. 191, Photometric Redshifts and the Detection of High Redshift Galaxies, ed. R. Weymann, L. Storrie-Lombardi, M. Sawicki, & R. Brunner (San Francisco, CA: ASP), 229
Dickinson, M., Stern, D., Giavalisco, M., et al. 2004, ApJ, 600, L99
Douglas, L. S., Bremer, M. N., Lehnert, M. D., Stanway, E. R., & Milvang-Jensen, B. 2010, MNRAS, 409, 1155
Dressler, A., Bigelow, B., Hare, T., et al. 2011, PASP, 123, 288
Dunkley, J., Komatsu, E., Nolta, M. R., et al. 2009, ApJS, 180, 306
Ellis, R., Santos, M. R., Kneib, J.-P., & Kuijken, K. 2001, ApJ, 560, L119
Fan, X., Carilli, C. L., & Keating, B. 2006, ARA&A, 44, 415
Fan, X., Narayanan, V. K., Strauss, M. A., et al. 2002, AJ, 123, 1247
Hamuy, M., Suntzeff, N. B., Heathcote, S. R., et al. 1994, PASP, 106, 566
Harris, W. E. 1991, ARA&A, 29, 543
Hippelein, H., Maier, C., Meisenheimer, K., et al. 2003, A&A, 402, 65
Hu, E. M., Cowie, L. L., Barger, A. J., et al. 2010, ApJ, 725, 394
Hu, E. M., Cowie, L. L., Capak, P., et al. 2004, AJ, 127, 563
Inoue, A. K., Kousai, K., Iwata, I., et al. 2011, MNRAS, 411, 2336
Iwata, I., Inoue, A. K., Matsuda, Y., et al. 2009, ApJ, 692, 1287
Kashikawa, N., Shimasaku, K., Malkan, M. A., et al. 2006, ApJ, 648, 7
Kashikawa, N., Shimasaku, K., Matsuda, Y., et al. 2011, ApJ, 734, 119
Komatsu, E., Dunkley, J., Nolta, M. R., et al. 2009, ApJS, 180, 330
Landy, S. D., & Szalay, A. S. 1993, ApJ, 412, 64
Lehnert, M. D., & Bremer, M. 2003, ApJ, 593, 630
Lemaux, B. C., Lubin, L. M., Sawicki, M., et al. 2009, ApJ, 700, 20
Loveday, J., Peterson, B. A., Efstathiou, G., & Maddox, S. J. 1992, ApJ, 390, 338
Ly, C., Malkan, M. A., Kashikawa, N., et al. 2007, ApJ, 657, 738
Madau, P., Haardt, F., & Rees, M. J. 1999, ApJ, 514, 648
Malhotra, S., & Rhoads, J. E. 2002, ApJ, 565, L71
Malhotra, S., & Rhoads, J. E. 2004, ApJ, 617, L5
Malkan, M., Webb, W., & Konopacky, Q. 2003, ApJ, 598, 878
Martin, C. L., & Sawicki, M. 2004, ApJ, 603, 414
Martin, C. L., Sawicki, M., Dressler, A., & McCarthy, P. 2008, ApJ, 679, 942
Martin, C. L., Scannapieco, E., Ellison, S. L., et al. 2010, ApJ, 721, 174
Marzke, R., McCarthy, P. J., Persson, E., et al. 1999, in ASP Conf. Ser. 191, Photometric Redshifts and the Detection of High Redshift Galaxies, ed. R. Weymann, L. Storrie-Lombardi, M. Sawicki, & R. Brunner (San Francisco, CA: ASP), 148
Marzke, R. O., Geller, M. J., Huchra, J. P., & Corwin, H. G., Jr. 1994, AJ, 108, 437
Meurer, G. R., Heckman, T. M., & Calzetti, D. 1999, ApJ, 521, 64
Miyazaki, S., Komiyama, Y., Sekiguchi, M., et al. 2002, PASJ, 54, 833
Murayama, T., Taniguchi, Y., Scoville, N. Z., et al. 2007, ApJS, 172, 523
Nestor, D. B., Shapley, A. E., Steidel, C. C., & Siana, B. 2011, ApJ, 736, 18
Ouchi, M., Shimasaku, K., Akiyama, M., et al. 2008, ApJS, 176, 301
Ouchi, M., Shimasaku, K., Furusawa, H., et al. 2010, ApJ, 723, 869
Page, L., Hinshaw, G., Komatsu, E., et al. 2007, ApJS, 170, 335
Pawlik, A. H., Schaye, J., & van Scherpenzeel, E. 2009, MNRAS, 394, 1812
Rauch, M., Haehnelt, M., Bunker, A., et al. 2008, ApJ, 681, 856
Salvaterra, R., Ferrara, A., & Dayal, P. 2011, MNRAS, 414, 847
Santos, M. R., Ellis, R. S., Kneib, J.-P., Richard, J., & Kuijken, K. 2004, ApJ, 606, 683
Sawicki, M., Lemaux, B. C., Guhathakurta, P., et al. 2008, ApJ, 687, 884
Schaerer, D. 2002, A&A, 382, 28
Schaerer, D., & Charbonnel, C. 2011, MNRAS, 413, 2297
Schechter, P. 1976, ApJ, 203, 297
Scoville, N., Aussel, H., Brusa, M., et al. 2007, ApJS, 172, 1
Shapley, A. E., Steidel, C. C., Pettini, M., & Adelberger, K. L. 2003, ApJ, 588, 65
Shapley, A. E., Steidel, C. C., Pettini, M., Adelberger, K. L., & Erb, D. K. 2006, ApJ, 651, 688
Shimasaku, K., Kashikawa, N., Doi, M., et al. 2006, PASJ, 58, 313
Shioya, Y., Taniguchi, Y., Sasaki, S. S., et al. 2008, ApJS, 175, 128
Siana, B., Teplitz, H. I., Colbert, J., et al. 2007, ApJ, 668, 62
Siana, B., Teplitz, H. I., Ferguson, H. C., et al. 2010, ApJ, 723, 241
Spergel, D. N., Bean, R., Doré, O., et al. 2007, ApJS, 170, 377
Stanway, E. R., Bunker, A. J., Glazebrook, K., et al. 2007, MNRAS, 376, 727
Stanway, E. R., Bunker, A. J., & McMahon, R. G. 2003, MNRAS, 342, 439
Stark, D. P., Ellis, R. S., Chiu, K., Ouchi, M., & Bunker, A. 2010, MNRAS, 408, 1628
Stark, D. P., Ellis, R. S., & Ouchi, M. 2011, ApJ, 728, L2
Steidel, C. C., Bogosavljević, M., Shapley, A. E., et al. 2011, ApJ, 736, 160
Steidel, C. C., Pettini, M., & Adelberger, K. L. 2001, ApJ, 546, 665
Stewart, K. R., Bullock, J. S., Wechsler, R. H., Maller, A. H., & Zentner, A. R. 2008, ApJ, 683, 597
Stubbs, C. W., & Tonry, J. L. 2006, ApJ, 646, 1436
Takahashi, M. I., Shioya, Y., Taniguchi, Y., et al. 2007, ApJS, 172, 456
Taniguchi, Y., Scoville, N., Murayama, T., et al. 2007, ApJS, 172, 9
Tran, K.-V. H., Lilly, S. J., Crampton, D., & Brodwin, M. 2004, ApJ, 612, L89
Trenti, M., Stiavelli, M., Bouwens, R. J., et al. 2010, ApJ, 714, L202
Vanzella, E., Giavalisco, M., Inoue, A. K., et al. 2010, ApJ, 725, 1011
Yan, H., & Windhorst, R. A. 2004, ApJ, 612, L93